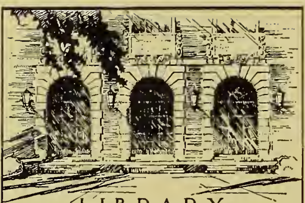

ANTENNA LABORATORY

Technical Report No. 36

USE OF COUPLED WAVEGUIDES IN A TRAVELING WAVE SCANNING ANTENNA

by

Robert Henry MacPhie*

30 April 1959

Contract AF33(616)-6079
Project No. 9-(13-6278) Task 40572

Sponsored by:

WRIGHT AIR DEVELOPMENT CENTER

Electrical Engineering Research Laboratory
Engineering Experiment Station
University of Illinois
Urbana, Illinois

---

*Submitted in partial fulfillment of the requirements for the degree of Master of Science in Electrical Engineering at the University of Illinois, 1959.

ACKNOWLEDGMENTS

It is a pleasure to acknowledge the large measure of advice and encouragement given by Dr. Weeks on whose suggestion (Appendix D of Reference 3) the experimental work was based. Discussions with Professor Deschamps were always helpful. T. Lahey was of invaluable service in the calculation of the theoretical radiation patterns. Thanks are due also to G. Powers and V. Beinekis for their assistance in the experimental work.

ABSTRACT

An array of closely-spaced transverse slots, cut in the broad wall of a rectangular waveguide, and set flush with a large ground plane is used as the radiating aperture of a traveling wave scanning antenna. The waveguide is coupled by circular holes in its other broad wall to a second waveguide which is identical except that it lacks radiating slots. The coupled system permits two normal modes of propagation in the waveguides whose phase velocities differ and whose relative amplitudes can be controlled by a phase shifter. Since the angle ϕ which a traveling wave antenna's main lobe makes with its axis is given by $\phi = \cos^{-1} \frac{c}{v}$, where c is the velocity of light and v is the phase velocity along the antenna, there will be two main lobes at $\phi_F = \cos^{-1} \frac{c}{v_F}$ and $\phi_S = \cos^{-1} \frac{c}{v_S}$ where v_F is the phase velocity of the fast mode and v_S is that of the slow mode. The relative amplitudes of the lobes can be controlled and this effectively produces a scan from ϕ_F to ϕ_S. This report describes an antenna that scans in the end-fire region. The two cases considered have scans from $\phi = 0^\circ$ (end fire) to $\phi = 23^\circ$ and from $\phi = 12^\circ$ to $\phi = 30^\circ$. The aperture length in both cases is approximately ten wavelengths. The scan is continuous, but the beam amplitude varies considerably and efficiency is low. The antenna design, however, is relatively simple requiring only one phase shifting device which may be electronic.

CONTENTS

ILLUSTRATIONS

ILLUSTRATIONS (CONTINUED)

LIST OF SYMBOLS

V_1, V_2,	transverse voltages on a pair of coupled transmission lines.
I_1, I_2,	currents on the coupled transmission lines.
Z_{11}, Z_{22},	impedances per unit length on the transmission lines.
Y_{11}, Y_{22},	admittances per unit length on the transmission lines.
Z_{12}, Z_{21},	coupling impedances per unit length on the transmission lines.
Y_{12}, Y_{21},	coupling admittances per unit length on the transmission lines.
z,	distance on the lines from start of coupling.
β_F,	propagation constant of the faster mode of propagation on the coupled transmission lines.
β_S,	propagation constant of the slower mode of propagation on the coupled transmission lines.
β_1, β_2, c_{12}, c_{21},	constants used to define β_F and β_S in terms of the coupled transmission line parameters and defined in Part I, Equation (5).
β_a,	average propagation constant ($\beta_a = \frac{\beta_S + \beta_F}{2}$).
β_b,	beat propagation constant ($\beta_b = \frac{\beta_S - \beta_F}{2}$).
θ	relative phase angle between incident transverse voltages V_1, V_2, at $z = 0$, the start of coupling.
λ_b,	beat wavelength ($\lambda_b = \frac{2\pi}{\beta_b}$).
ϕ,	radiation angle measured from the z axis, the axis of the aperture.
$E_{(\phi)}$,	far electric field strength radiated from the aperture.
$E_{AP(z)}$,	aperture electric field strength (tangential).
β_o,	free space propagation constant.
$L_2 - L_1 = L$,	length of radiating aperture.

SYMBOLS CONTINUED

ϕ_F,	main lobe radiation angle of fast normal mode.
ϕ_S,	main lobe radiation angle of slow normal mode.
v_F,	phase velocity of the fast mode of propagation.
v_S,	phase velocity of the slow mode of propagation.
$\psi_{\substack{F\\S}}$,	parameter in radiation pattern $(\psi_{\substack{F\\S}} = \frac{\pi L}{\lambda_o}[\frac{c}{v_{\substack{F\\S}}} - \cos\phi])$
a,	width of rectangular waveguide
b,	height of rectangular waveguide.
d,	depth of dielectric filling in rectangular waveguide.
c,	velocity of light.
f,	frequency in cycles per second.
ω,	angular frequency in radians per second.
v_U,	phase velocity in uncoupled waveguide.
λ_o	wavelength in free space $(\lambda_o = \frac{c}{f})$.
j,	complex operator $= \sqrt{-1}$,

INTRODUCTION

The theory of coupled waveguides from the exact, i.e., Maxwellian viewpoint, is indeed difficult. (This is due to the non-separable nature of the coordinates of the coupled system; see Figure 1). Because of this, most theoretical attacks employ variational methods or other techniques such as Floquet's theorem[1] to get useful results. Happily, the design of this type of antenna does not require a solution of the boundary value problem. It is sufficient to know the variation in the field as a function of distance down the waveguides. Maxwell's equations can be replaced by the ordinary differential equations of coupled transmission lines[1]. The solution of these equations for the voltage on either line can be used as an analogue of the solution for the electric field as a function of distance along the corresponding waveguide.

The voltage (or electric field) is in terms of two normal modes having different phase velocities. Their mathematical representation is quite familiar, since the expressions are identical to those obtained from the coupled pendula or spring-mass problems.[2] The analogue is such that time, as the independent variable in the latter cases, corresponds to distance in the waveguide-transmission line case.

The following is an outline of the design procedure. Two identical uncoupled waveguides are built; their dominant mode phase velocity is approximately equal to that which will give the specified direction of main lobe radiation. For example, if the scan is to be in the end fire region, v_U, the phase velocity of the uncoupled waveguides must be slightly greater than c. (One uses the formula $\phi = \cos^{-1} \frac{c}{v}$.) The coupling holes in a

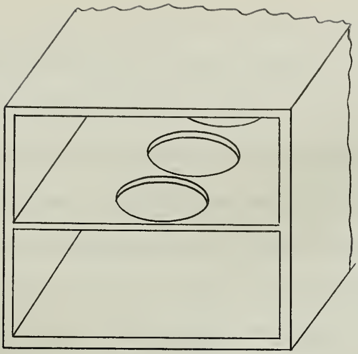

FIGURE 1 COUPLED WAVEGUIDES

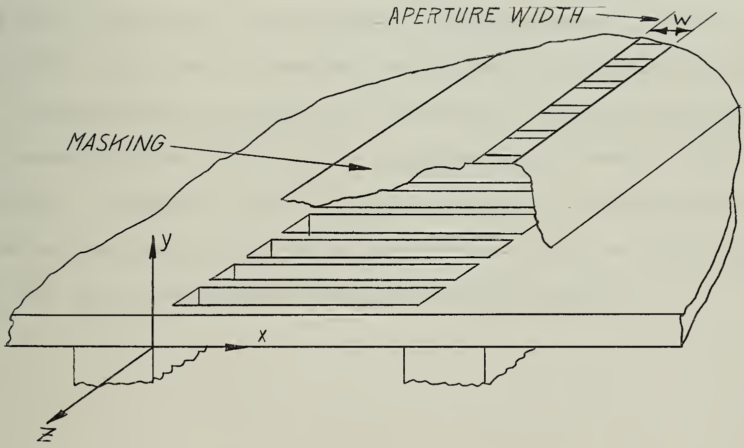

FIGURE 2 RADIATING APERTURE AND MASKING

common broad wall are then introduced and their size and spacing is varied on a cut-and-try basis until the correct amount of coupling is obtained. This is determined by using the mode theory of the transmission line analogue to interpret the observed variation in field strength along the waveguides. The analogue is also used to predict the main features of the radiation patterns. Radiation is obtained from a large number of slots which are subsequently cut in the top wall of the upper waveguide; it is confined to a half space by a large ground plane, Figure 2. The main lobe of the radiation pattern is in the end fire region where a given change in phase velocity causes the greatest scan, i.e., $d \cos (c/v)/dv$ has a maximum at $c/v = 1$ or $\phi = 0^{\circ}$.

Two separate scans were obtained. The first was from $\phi = 0^{\circ}$ (endfire) to $\phi = 23^{\circ}$; the second, with a different coupling aperture, was from $\phi = 12^{\circ}$ to $\phi = 30^{\circ}$. The effect of frequency and aperture size was also investigated.

This manuscript is divided into three parts. Part one will present the transmission line theory and the radiation pattern theory. This is essentially a resumé of a report[3] by W. L. Weeks. In the second part details of the antenna design and measuring apparatus will be given. Part three will deal with the experimental work and its interpretation.

1. THEORY

1.1 The Coupled Transmission Line Analogy

Coupled transmission lines are considered to be the analogue of the coupled waveguides of Figure 1. The coupling holes which transfer energy from one waveguide to the other determine the coupling impedances and admittances in the following coupled transmission line differential equations,

$$\frac{dV_1}{dz} = -Z_{11} I_1 + Z_{12} I_2 \qquad \frac{dI_1}{dz} = -Y_{11} V_1 + Y_{12} V_2 \tag{1}$$

$$\frac{dV_2}{dz} = -Z_{22} I_2 + Z_{21} I_1 \qquad \frac{dI_2}{dz} = -Y_{22} V_2 + Y_{21} V_1 \tag{2}$$

where V_1 = transverse voltage on line 1,

V_2 = transverse voltage on line 2,

I_1 = current on line 1,

I_2 = current on line 2,

Z_{11} = impedance per unit length of line 1,

Z_{22} = impedance per unit length of line 2,

Y_{11} = admittance per unit length of line 1,

Y_{22} = admittance per unit length of line 2,

Z_{12} = coupling impedance per unit length between line 1 and line 2,

Z_{21} = coupling impedance per unit length between line 2 and line 1,

Y_{12} = coupling admittance per unit length between line 1 and line 2,

Y_{21} = coupling admittance per unit length between line 2 and line 1,

z = distance on the line from the start of coupling.

Solution[1] of these equations leads to the following expressions for the transverse voltage, provided the backward traveling waves are negligible:

$$\begin{aligned} V_1 &= V_{1F}\, e^{-j\beta_F z} + V_{1S}\, e^{-j\beta_S z} \\ V_2 &= V_{2F}\, e^{-j\beta_F z} + V_{2S}\, e^{-j\beta_S z} \end{aligned} \qquad (3)$$

where

$$\begin{aligned} \beta_F &= \left| \left\{ \tfrac{1}{2}(\beta_1^{\,2} + \beta_2^{\,2}) - \tfrac{1}{2}\sqrt{(\beta_1^{\,2} - \beta_2^{\,2})^2 + 4c_{12}^{\,2}\, c_{21}^{\,2}} \right\}^{\frac{1}{2}} \right| \\ \beta_S &= \left| \left\{ \tfrac{1}{2}(\beta_1^{\,2} + \beta_2^{\,2}) + \tfrac{1}{2}\sqrt{(\beta_1^{\,2} - \beta_2^{\,2})^2 + 4c_{12}^{\,2}\, c_{21}^{\,2}} \right\}^{\frac{1}{2}} \right| \end{aligned} \qquad (4)$$

and

$$\begin{aligned} \beta_1^{\,2} &= Z_{11} Y_{11} + Z_{12} Y_{21} \\ \beta_2^{\,2} &= Z_{22} Y_{22} + Z_{21} Y_{12} \\ c_{12}^{\,2} &= Z_{11} Y_{12} + Z_{12} Y_{22} \\ c_{21}^{\,2} &= Z_{21} Y_{11} + Z_{22} Y_{21} \,. \end{aligned} \qquad (5)$$

β_F is the propagation constant of the faster mode of propagation and β_S is the propagation constant of the slower mode. This formulation assumes that propagation is without loss.

If the two transmission lines (waveguides) are identical, the above expressions are considerably simplified.

$$\beta_1 = \beta_2 \qquad \text{and} \qquad c_{12} = c_{21} = c_o$$

Thus

$$\beta_F = \left|(\beta_a{}^2 - c_o{}^2)^{\frac{1}{2}}\right| \qquad \beta_S = \left|(\beta_a{}^2 + c_o{}^2)^{\frac{1}{2}}\right| \tag{6}$$

Where

$$\beta_a = \frac{\beta_1 + \beta_2}{2} = \beta_1 = \beta_2$$

is called the average propagation constant. Since relatively weak coupling is used ($c_o \ll \beta_a$), Equation (6) can be approximated by the first two terms of the binomial expansion as follows:

$$\beta_F \simeq \left|\beta_a - \frac{1}{2}\frac{c_o{}^2}{\beta_a}\right| = \left|\beta_a - \beta_b\right| \qquad \beta_S \simeq \left|\beta_a + \frac{1}{2}\frac{c_o{}^2}{\beta_a}\right| = \left|\beta_a + \beta_b\right| \tag{7}$$

where

$$\beta_b = \frac{c_o{}^2}{2\beta_a}$$

is called the beat propagation constant. Equations (7) show that the normal mode propagation constants β_F and β_S can, on such transmission lines, be thought of as an average β_a and the difference or sum of this with a much smaller quantity β_b. Note that this smaller quantity is a measure of the separation of the two normal mode phase velocities and it follows from (7) that strong coupling (large c_o) causes large separation.

The coefficients V_{1F} etc. in Equation (3) are functions of the amplitudes and phase of the voltages across the two transmission lines at the beginning of coupling, z = 0, and for uniform, infinite (or matched) lines are independent of all other factors. This therefore is an initial value

[illegible]

$$[illegible]$$

[illegible]

$$[illegible]$$

[illegible]

$$[illegible]$$

$$[illegible]$$

[illegible]

problem, In an idealized pair of transmission lines (waveguides) the following conditions will obtain:

a) the lines will be identical,

b) the incident fields at $z = 0$ will be equal in amplitude and differ only by an arbitrary phase angle θ. Thus, if $V_2(0)$ is normalized at 1, $V_1(0)$ can be denoted simply by $e^{j\theta}$. This gives the following expressions for the line voltages (or waveguide electric fields) as a function of z and θ.

$$V_1 = \left[\frac{1+e^{j\theta}}{2}\right] e^{-j\beta_F z} - \left[\frac{1-e^{j\theta}}{2}\right] e^{-j\beta_S z} \qquad (8)$$
$$V_2 = \left[\frac{1+e^{j\theta}}{2}\right] e^{-j\beta_F z} + \left[\frac{1-e^{j\theta}}{2}\right] e^{-j\beta_S z}$$

or

$$V_1 = e^{j\frac{\theta}{2}} \left[\cos\left(\frac{\theta}{2}\right) e^{-j\beta_F z} + j \sin\left(\frac{\theta}{2}\right) e^{-j\beta_S z}\right] \qquad (9)$$
$$V_2 = e^{j\frac{\theta}{2}} \left[\cos\left(\frac{\theta}{2}\right) e^{-j\beta_F z} - j \sin\left(\frac{\theta}{2}\right) e^{-j\beta_S z}\right]$$

This can also be written as

$$V_1 = e^{j\frac{\theta}{2}} \left[\cos\frac{\theta}{2} + j \sin\frac{\theta}{2}\, e^{-j2\beta_b z}\right] e^{-j\beta_F z} \qquad (10)$$
$$V_2 = e^{j\frac{\theta}{2}} \left[\cos\frac{\theta}{2} - j \sin\frac{\theta}{2}\, e^{-j2\beta_b z}\right] e^{-j\beta_F z}$$

Equations (10) are used in Figure 3 to show phasorially the variation of the amplitude and phase of V_1 and V_2 for different values of z and an arbitrary value of θ $(= \frac{\pi}{4})$. The phasor $e^{-j\beta_F z}$ is taken as a reference. It can be seen that the amplitude of the line voltages varies considerably with z.

$$V_1 = e^{j\theta}\left[\cos\left(\frac{\theta}{2}\right) + j\sin\left(\frac{\theta}{2}\right) j e^{-j2\beta_b z}\right] e^{-j\beta_F z}$$

$$V_2 = e^{j\theta}\left[\cos\left(\frac{\theta}{2}\right) - j\sin\left(\frac{\theta}{2}\right) e^{-j\beta_F z}\right] e^{-j\beta_F z}$$

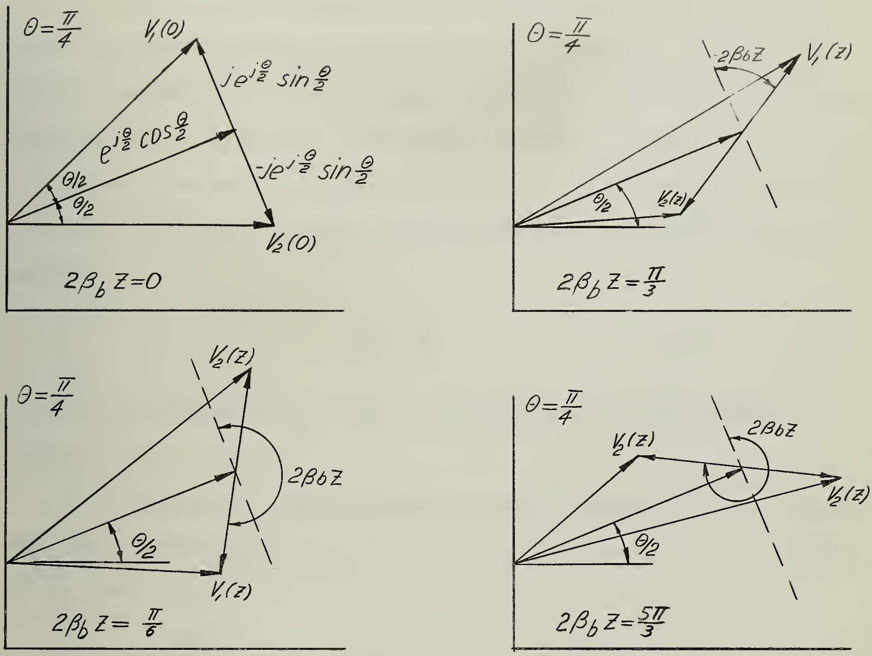

FIGURE 3 PHASOR DIAGRAMS OF TRANSMISSION LINE VOLTAGES $V_1(z)$ AND $V_2(z)$ FOR $\theta = \pi/4$, ($e^{-j\beta_F z}$ IS TAKEN AS A REFERENCE PHASOR).

Figure 4 shows this variation of amplitude for V_1 as a function of z for different values of the parameter Θ. Note that at $\Theta = 0^\circ$ and 180° there is no variation; this is because only one normal mode is excited in each case and there is consequently no interference phenomenon. At $\Theta = 90^\circ$ and 270° the two modes are excited equally (see Figure 5) and total cancellation occurs at regular intervals. The distance between two minima of V_1 for any Θ turns out to be related to β_b of Equation (7). This distance is one half of what will be called the beat wavelength which is given by the following equation*

$$\lambda_b = \frac{2\pi}{\beta_b} \tag{11}$$

The minima and maxima occur at $\frac{\lambda_b}{8} + n\frac{\lambda_b}{4}$ from z = 0, the beginning of coupling, n = 0, 1, 2, 3, ...

It proved helpful in the experimental work to study the field variations when one waveguide had no incident field at z = 0. For this case the fields can be shown to be

$$V_1 = \sin \beta_b Z \, e^{-j\beta_a z}, \quad V_2 = \cos \beta_b Z \, e^{-j\beta_a z}, \quad \text{if } V_1\Big|_{z=0} = 0 \quad V_2\Big|_{z=0} = 1,$$

or (12)

$$V_1 = \cos \beta_b Z \, e^{-j\beta_a z}, \quad V_2 = \sin \beta_b Z \, e^{-j\beta_a z}, \quad \text{if } V_1\Big|_{z=0} = 1 \quad V_2\Big|_{z=0} = 0.$$

These curves are shown in Figure 6. It is evident that a phased combination of these produced the more complicated effects shown in Figure 4.

---

* This defines λ_b as being equal to twice the usual "beat wavelength" found in the literature.

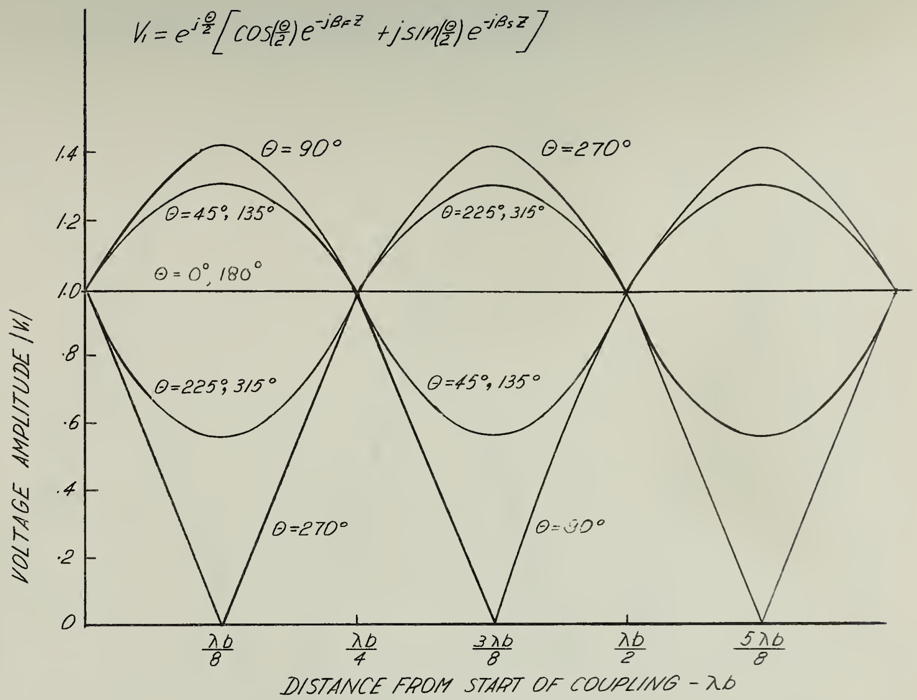

FIGURE 4 VOLTAGE AMPLITUDE VS. DISTANCE FROM START OF COUPLING WITH DIFFERENT VALUES OF THE PARAMETER Θ.

$$V_1 = e^{j\frac{\Theta}{2}}\left[\cos\left(\frac{\Theta}{2}\right)e^{-j\beta_F Z} + j\sin\left(\frac{\Theta}{2}\right)e^{-j\beta_S Z}\right] = V_F + V_S$$

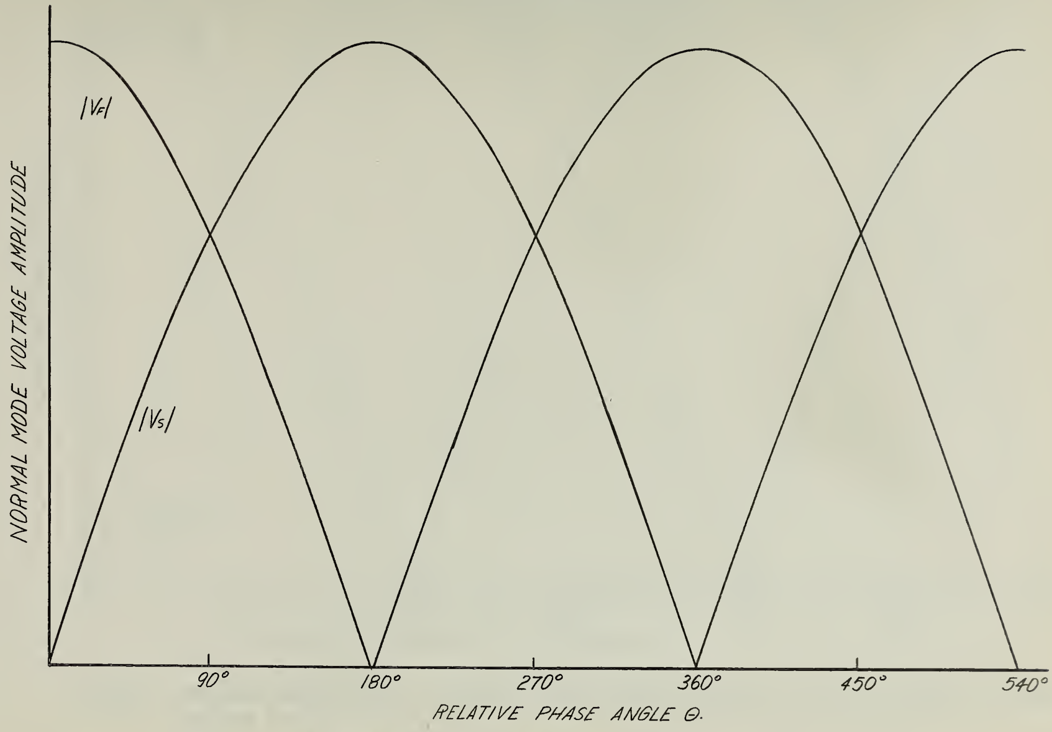

FIGURE 5 NORMAL MODE VOLTAGE AMPLITUDE VS. RELATIVE PHASE ANGLE Θ

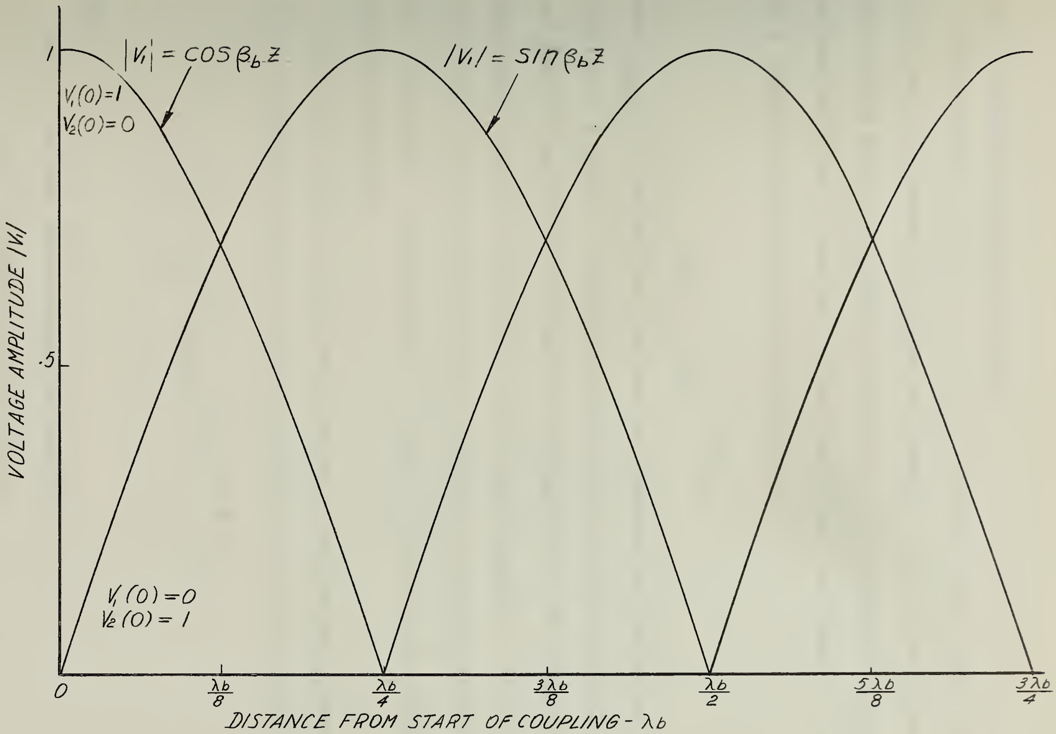

FIGURE 6 VOLTAGE AMPLITUDE VS. DISTANCE FROM START OF COUPLING WITH NO INCIDENT VOLTAGE ON ONE LINE.

1.2 The Antenna Aperture and Pattern

The radiating aperture is an array of closely-spaced non-resonant slots cut in the upper broad wall of the top waveguide which is set flush in a large ground plane as is shown in Figure 2. In the theory it is assumed that the aperture field is constant in the x direction (see Figure 2), and that the z variation is of the traveling wave type, i.e.,

$$E_{AP}(z) = K_{(z\theta)}\, e^{-j\beta_{(\theta z)} z}$$

where $\beta_{(\theta z)} z$ is obtained from the coupled transmission line analogy and is a function of θ and z.* The power loss per unit length due to radiation is kept small enough so that the modes of propagation in the waveguides are not appreciably different from those in the closed waveguides. In the experimental work this loss was controlled by masking the aperture with aluminum foil. As a result the attenuation of $E_{AP}(z)$ will be omitted from the theoretical expressions.

The large number of slots (over twelve per wavelength) allows one to use the continuous aperture integral expression for the far field;

$$E_{(\phi)} = \int_{L_1}^{L_2} E_{AP(z)}\, e^{+j\beta_o \cos\phi\, z}\, dz, \qquad (13)$$

where

β_o = free space propagation constant,

$L_2 - L_1$ = L, the length of the aperture,

ϕ = radiation angle measured from the z axis, the axis of the aperture (see Figure 7),

---

* See Appendix A

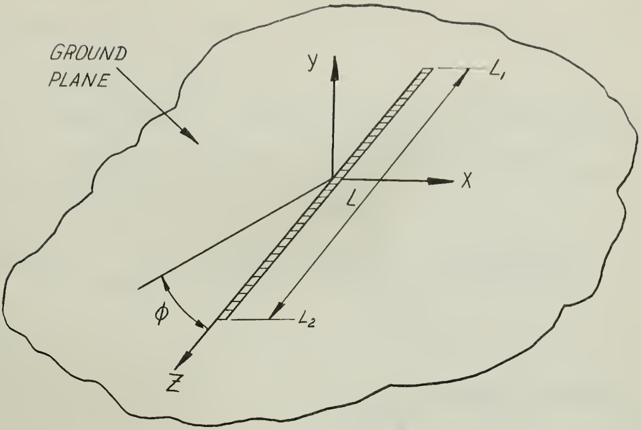

FIGURE 7 APERTURE AND COORDINATE SYSTEM

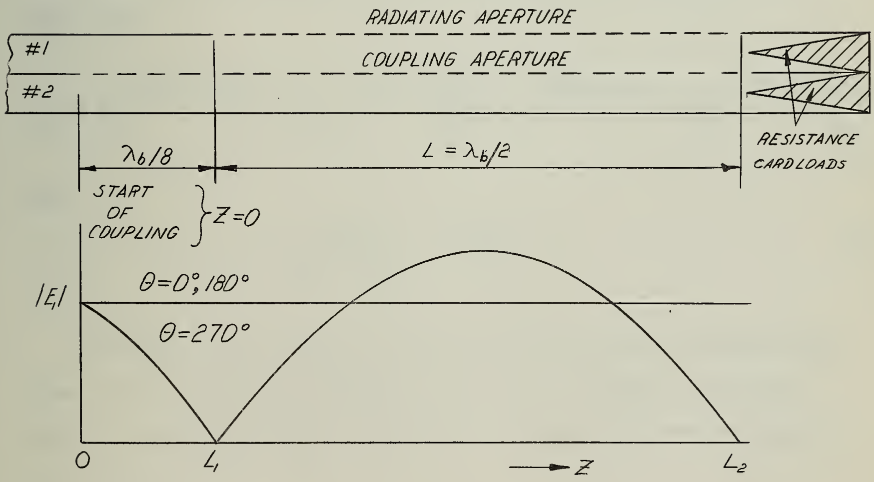

FIGURE 8 LOCATION OF RADIATING APERTURE RELATIVE TO COUPLING APERTURE

$E_{AP(z)}$ = aperture field strength, proportional to the field strength in the upper waveguide, E_1.

But E_1 can be expressed by its transmission line analogue, Equation (9). Hence, except for a constant of proportionality between E_1 and $E_{AP(z)}$, the integral equation (13) can be written as follows:

$$E_{(\phi)} = \int_{L_1}^{L_2} e^{j[\frac{\theta}{2} - \beta_F L_1]} \left\{ \cos\frac{\theta}{2}\, e^{-j(\beta_F - \beta_o \cos\phi) z} \right\} dz + j \int_{L_1}^{L_2} e^{j[\frac{\theta}{2} - \beta_S L_1]} \left\{ \sin\frac{\theta}{2}\, e^{-j(\beta_S - \beta_o \cos\phi) z} \right\} dz \qquad (14)$$

The total field is the sum of the two integrals associated with the two normal modes in the waveguides. These integrals have solutions of the $\frac{\sin\psi}{\psi}$ type:

$$E_{(\phi)} = \frac{L}{2} \left[e^{j[\frac{\theta}{2} - \beta_F L_1]} \cos\frac{\theta}{2}\, e^{-j\psi_F} \frac{\sin\psi_F}{\psi_F} + j e^{j(\frac{\theta}{2} - \beta_S L_1)} \sin\frac{\theta}{2}\, e^{-j\psi_S} \frac{\sin\psi_S}{\psi_S} \right] \qquad (15)$$

where

$$\psi_{\substack{F\\S}} = \frac{\pi L}{\lambda_o} \left[\frac{c}{v_{\substack{F\\S}}} - \cos\phi \right] \qquad (16)$$

Note that at $\theta = 0^\circ$, $\sin\frac{\theta}{2} = 0$, and the field is due to the fast mode alone. At $\theta = 180^\circ$ the slow mode alone exists to produce the radiated field. At other intermediate values of θ the total field is the phased sum of both.

2. ANTENNA DESIGN

2.1 Geometry of the Antenna

The location of the radiating aperture relative to the coupling aperture is shown in Figure 8. The start of coupling is $\lambda_b/8$ before the start of the radiating aperture at $z = L_1$. The length of the radiating aperture, $L = L_2 - L_1$, is $\lambda_b/2$. Also shown in Figure 8 is the amplitude of the upper waveguide field, i.e., the aperture field. Thus at a relative phase angle Θ equal to 0^o the aperture distribution is flat and according to Equations (15) and (16) the main lobe of the radiation pattern occurs at $\phi_F = \cos^{-1} \frac{c}{v_F}$. At $\Theta = -90^o$ or 270^o the aperture distribution is sinusoidal with a maximum in the center. This is known to give relatively low side lobes. The phase velocity is now $v_a = \frac{\omega}{\beta_a}$ and consequently $\phi_a = \cos^{-1} \frac{c}{v_a}$ is the new main lobe radiation angle. Finally, at $\Theta = 180^o$ the other normal mode, with a flat distribution in the aperture, will be excited and will cause a main lobe to be at $\phi_S = \cos^{-1} \frac{c}{v_a}$. This change in Θ of 180^o therefore causes a variation of the radiation angle of the main lobe, i.e., it causes a scan. The scan can be continuous with only a small variation in main lobe amplitude and with lower side lobes in the center of the scan. However, at $\Theta = 90^o$ the aperture distribution is cosinusoidal (recall Figure 4) with a null in the center and large side lobes are produced. Thus, a useful scan can be obtained (theoretically) by varying the relative phase of the two incident waveguide fields by only 180^o. It can also be shown that if the antenna aperture L is made much longer than $\lambda_b/2$ the two normal mode beams become so narrow that they do not overlap and the "scan" is reduced to a varying of the amplitudes of two lobes of constant angular separation. Thus the width of the lobe

has a lower bound approximately equal to the separation of the normal mode radiation angles ϕ_F and ϕ_S.

The design goal was an antenna whose beam could be scanned through an angle of about twenty degrees near end-fire. Therefore, if ϕ_S were 0^o (endfire) and ϕ_F were 26^o, then the variation in $\frac{c}{v}$ would be from 1.0 to 0.9 since $\phi = \cos^{-1} \frac{c}{v}$. The required separation of the two normal mode phase velocities would be about ten per cent.

This requirement also determines the length L of the aperture as follows:

$$L = \frac{\lambda_b}{2} = \frac{2\pi}{2\beta_b} = \frac{2\pi}{\beta_S - \beta_F} = \frac{v_F v_S}{f(v_F - v_S)}$$

and since $v_S \approx .9v_F$

$$L = \frac{.9v_F^{\,2}}{f(.1)v_F} = 9\lambda_F.$$

A nominal length of $10\lambda_o$ ($\lambda_o = \frac{c}{f}$) was taken as the design value for L. Figure 7 shows the aperture and coordinate system.

Since the coupling is weak, the phase velocity in each uncoupled waveguide is not appreciably changed when the holes are added. Thus, the uncoupled waveguides should have a dominant mode whose phase velocity v_U, is also slightly greater than that of light, i.e., $.9 < \frac{c}{v_U} < 1$. To obtain this relatively low v_U the waveguides are loaded with dielectric (polystyrene). This incidentally reduces the area of the waveguide cross section by about sixty per cent. Figure 9, taken from a report by Weeks,[4] shows the geometry of the waveguide cross section and its dielectric loading, together with a graph of $\frac{c}{v}$ vs. $\frac{\lambda_o}{2a}$ for different values of $\frac{d}{b}$, the dielectric fill ratio.

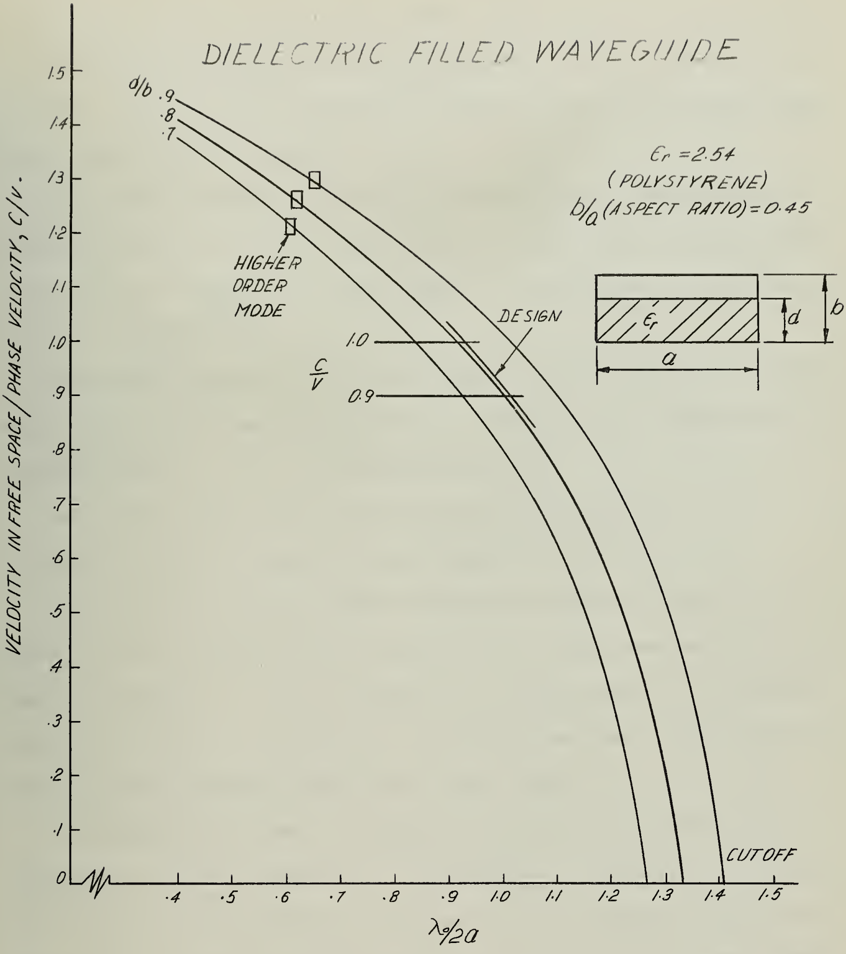

FIGURE 9 PHASE VELOCITY VARIATION IN DIELECTRIC FILLED WAVEGUIDE

A dielectric fill ratio $\frac{d}{b}$ of 0.81 is used. Thus, if $\frac{c}{v}$ is to vary from 0.9 to 1.0, the abscissa $\lambda_o/2a$ must vary from about 1.0 to 1.1. Note that the resulting design curve lies half way between cut off and the point where higher order modes are excited.

An arbitrary operating frequency of about eleven kilomegacycles per second was selected. With this and the above information, a scale drawing of the coupled waveguides was made, Figure 10. Also shown are the coupling and radiating apertures.

The coupling aperture is a row of large circular holes located on the center line of the common broad wall (see also Figure 1). There were two coupling apertures used in the experimental work.

No. 1, 5/16 inch diameter holes spaced 11/32 inch apart,

No. 2, 11/32 inch diameter holes spaced 3/8 inch apart.

The radiating aperture, whose dimensions are shown in Figure 10, is a number of narrow closely spaced transverse slots which have been used by a number of workers[5, 6, 7] and were shown to be quite suited to a traveling wave type of antenna. The amount of radiation from these slots is controlled by masking them with aluminum foil tape, Figure 2.

A diagram of the complete waveguide-antenna system employed in the experiments is shown in Figure 11. The antenna (a transmitter) is fed by a klystron; the usual attenuator, slotted line and frequency meter are in the circuit. A 3 db directional coupler feeds the klystron signal equally into two WR 90 waveguides in one of which is a phase shifter. A transition section connects the WR 90 waveguides to the smaller dielectric filled waveguides. The start of coupling $z = 0$, is a suitable distance beyond this transition. The coupling section is about 43 cm long (15 wavelengths).

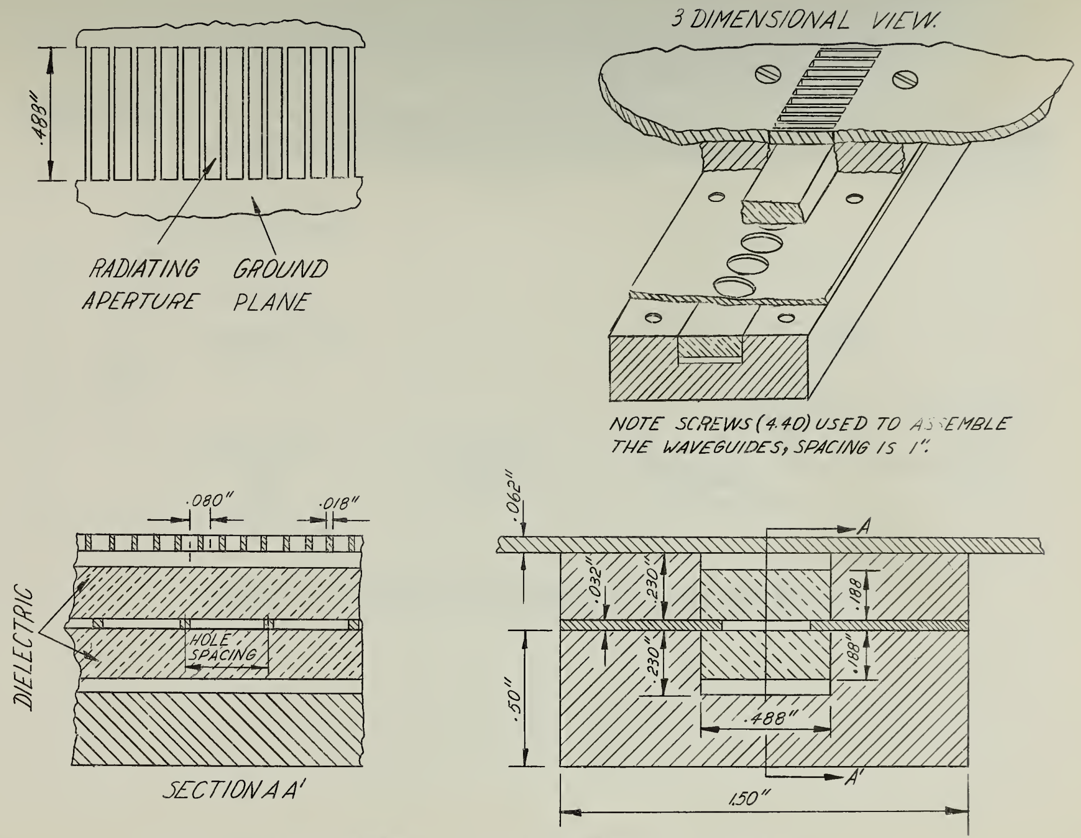

FIGURE 10 SCALE DRAWING OF THE COUPLED WAVEGUIDE ANTENNA

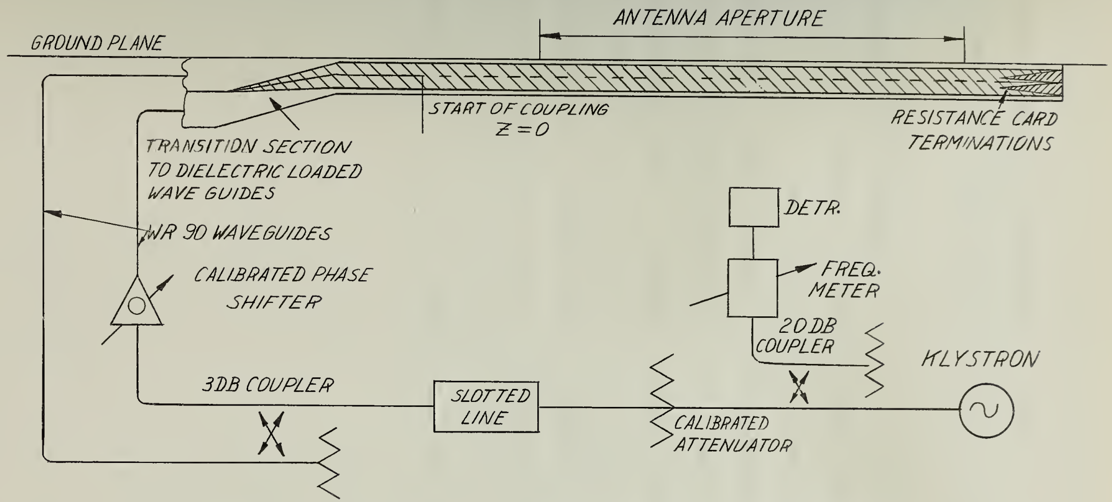

FIGURE 11 DIAGRAM OF THE COMPLETE WAVEGUIDE ANTENNA SYSTEM

As previously mentioned, the radiating aperture begins $\lambda_b/8$ after the start of coupling, is $\lambda_b/2$ in length and is mounted in a large ground plane. Resistance cards, located beyond the coupling aperture, minimize the reflected waves.

2.2 Antenna Pattern Range

Since the antenna is flush with a large ground plane, it radiates only into a half space. The actual geometry of the range for radiation pattern measurements is shown in Figure 12. The antenna is mounted at the center of the circular arc which forms part of the ground plane's perimeter. A small horn antenna mounted on a carriage responds to the component of electric field normal to the ground plane. This is recorded on a self-balancing potentiometer type recorder acting in conjunction with a selsyn drive system which draws the carriage along the circular periphery of the ground plane. The normal component of electric field, which is a function of ϕ, is measured for $0^\circ \leq \phi \leq 45^\circ$ on both sides of end-fire.

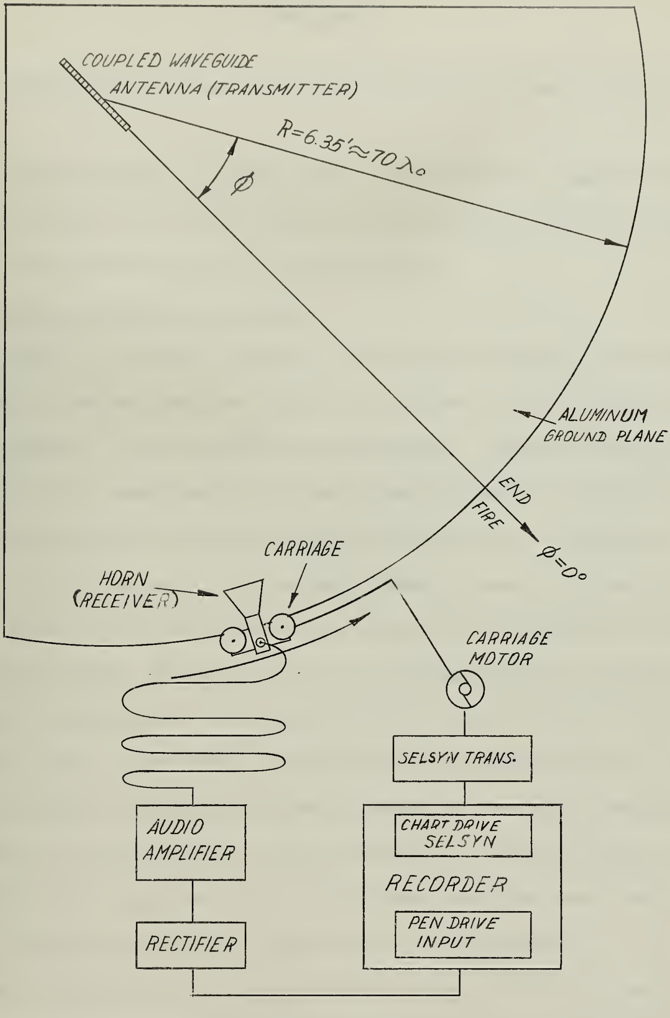

FIGURE 12 ANTENNA PATTERN RANGE

3. EXPERIMENT

The experimental work can be divided into three distinct parts as follows:

1) the investigation of the fields in non-radiating coupled waveguides,
2) the study of the effect of a radiating aperture on these fields,
3) the radiation patterns of this aperture.

3.1 Non-Radiating Coupled Waveguides

The fields in the upper waveguide were probed through a row of holes (.062 inch in diameter and .080 inch apart) drilled in its top wall, Figure 13. The radiation from these holes was negligible. Figure 14 shows the variation in field amplitude vs. distance from the start of coupling when energy is fed only to the lower waveguide (aperture no. 1 is used at a frequency of 11.20 kmc/sec). The energy gradually leaks into the upper waveguide (the transfer is total if the waveguides are identical) and then returns to the lower. The fact that this continues cyclically supports the transmission line analogy. Superposed on this large scale variation are smaller more rapid fluctuations, the usual standing wave patterns. A rough estimate of phase velocity can be made by measuring the guide wavelength. The presence of a standing wave implies negatively traveling waves, contrary to the theoretical assumption that only forward traveling waves exist. However, in most cases they are small enough to be negligible.

Since a relatively large number of such graphs will be reproduced, it will be advantageous to compress their size and omit the standing wave variation. Thus, in Figure 15, graph one is the reproduction of Figure 14. Graph two shows the opposite case of no incident field in the lower waveguide.

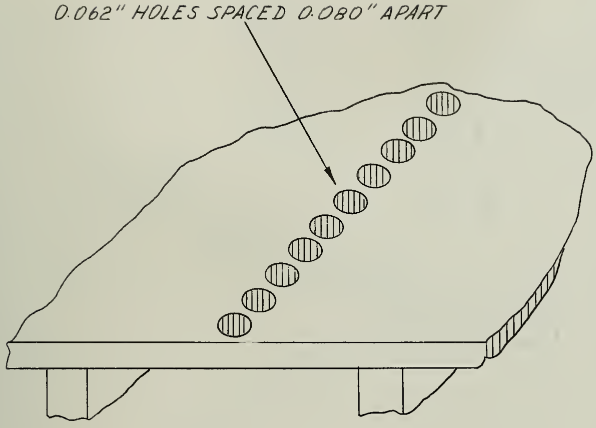

FIGURE 13 NON RADIATING WAVEGUIDE PROBING HOLES

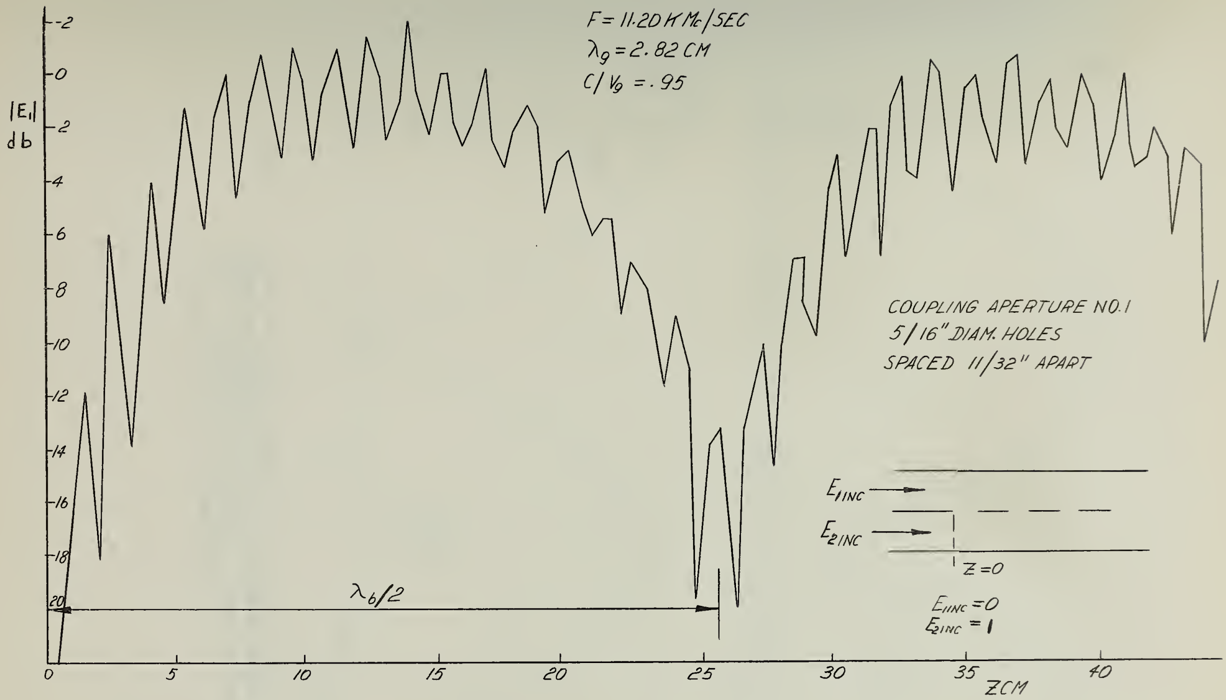

FIGURE 14 RELATIVE FIELD STRENGTH IN db VS. DISTANCE IN CM FROM START OF COUPLING WITH NO INCIDENT FIELD IN THE UPPER WAVEGUIDE, NON RADIATING CASE.

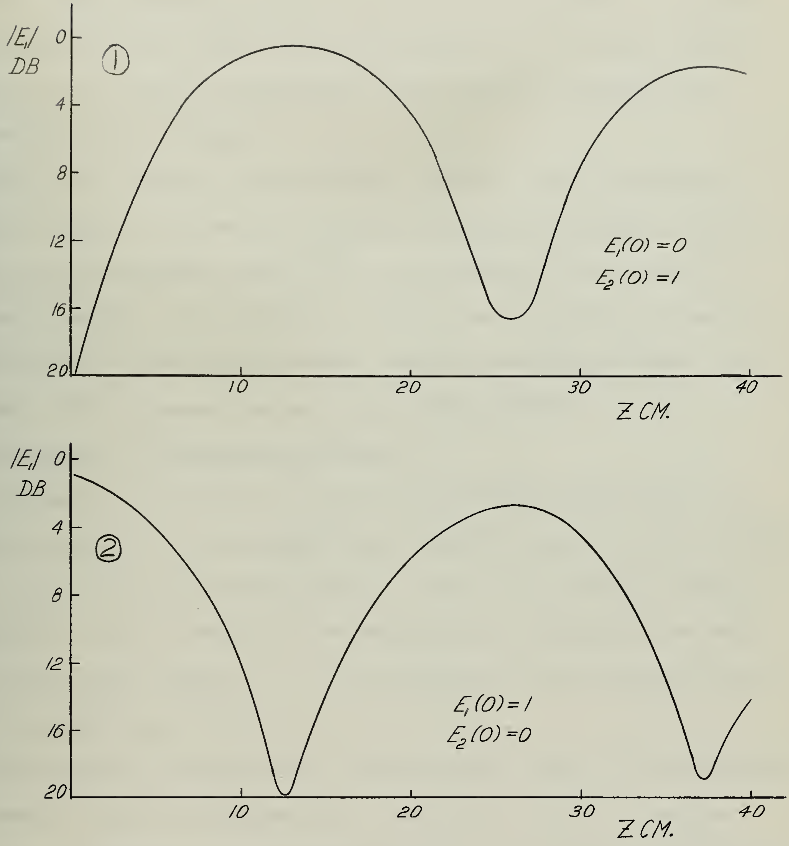

FIGURE 15 RELATIVE FIELD STRENGTH IN db VS. DISTANCE IN CM FROM START OF COUPLING WITH NO INCIDENT FIELD IN ONE WAVEGUIDE. NON-RADIATING CASE. COUPLING APERTURE NO. 1, F = 11.20 kmc/sec, EXPERIMENTAL.

These curves have their theoretical counterparts in Figure 6.

When both waveguides are excited and the relative phase θ is changed, the variation of the field in the upper waveguide is of the type shown in Figure 16. Note that the experimental curves closely approximate the theoretical curves of Figure 4.

At a lower frequency (11.00 kmc/sec) a similar set of results were obtained, Figure 17. Note that the beat wavelength is increased. This rather extreme frequency sensitivity of the coupling is illustrated in Figures 18 and 19. It is seen that a four per cent increase in frequency (10.8 kmc/sec to 11.2 kmc/sec) reduces the beat wavelength by about fifty per cent. This phenomenon was previously noted by Weeks.[3]

3.2 The Effect of the Radiating Aperture

Although the theoretical treatment of the problem assumed that the effect of radiation on the waveguide modes would be negligible, the aperture effect does disturb the fields somewhat. Thus it is necessary to limit radiation in order to retain the two normal modes of propagation on which the antenna theory depends, i.e., to retain aperture distributions similar to the non-radiating cases.

The effects of two apertures, 3/32 inch wide (.10λ_o) and 3/16 inch wide are shown in Figure 20 and Figure 21, respectively; the first coupling aperture at a frequency of 11.20 kmc/sec is used. Note that the 3/32 inch curves are quite similar to the non-radiating cases. However, there are distortions which are accentuated in the 3/16 inch case where radiation is greater. The beat wavelength is longer* (Figure 22) and the normal mode distributions are not as flat. The direct effect of radiation, the decreasing

---

* Appendix B is an analysis of this change.

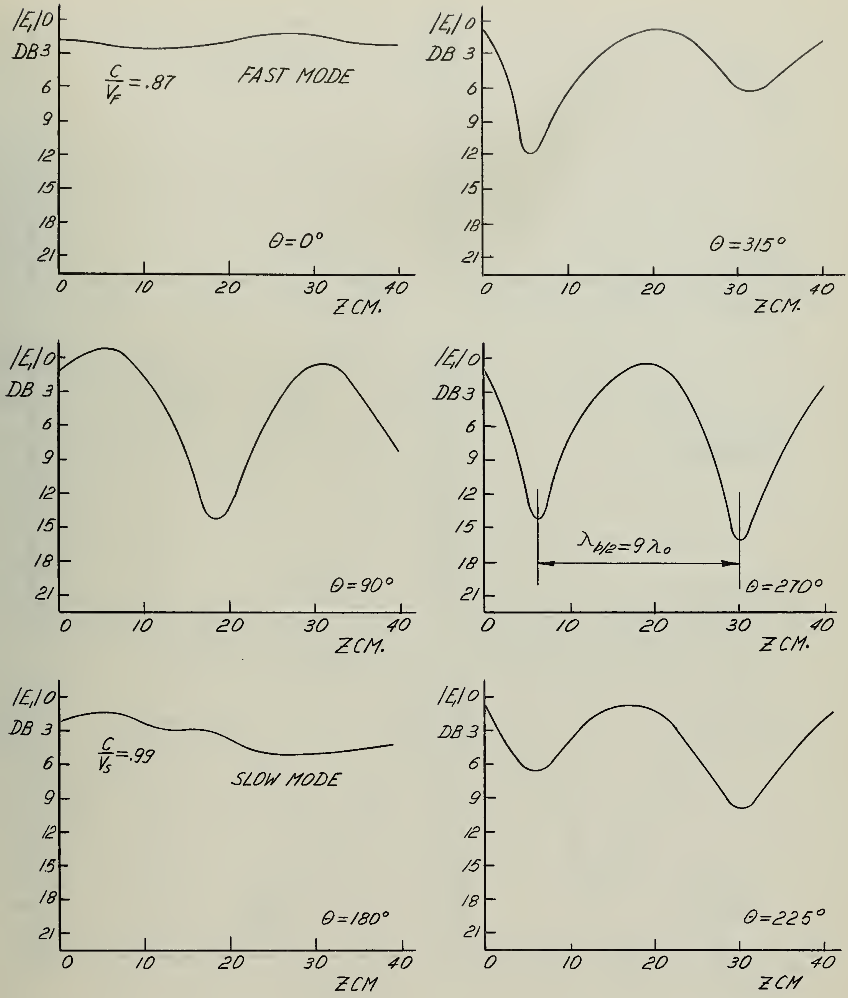

FIGURE 16 RELATIVE FIELD STRENGTH IN db VS. DISTANCE IN CM FROM START OF COUPLING. NON-RADIATING CASE, COUPLING APERTURE NO. 1, f = 11.20 kmc/sec .

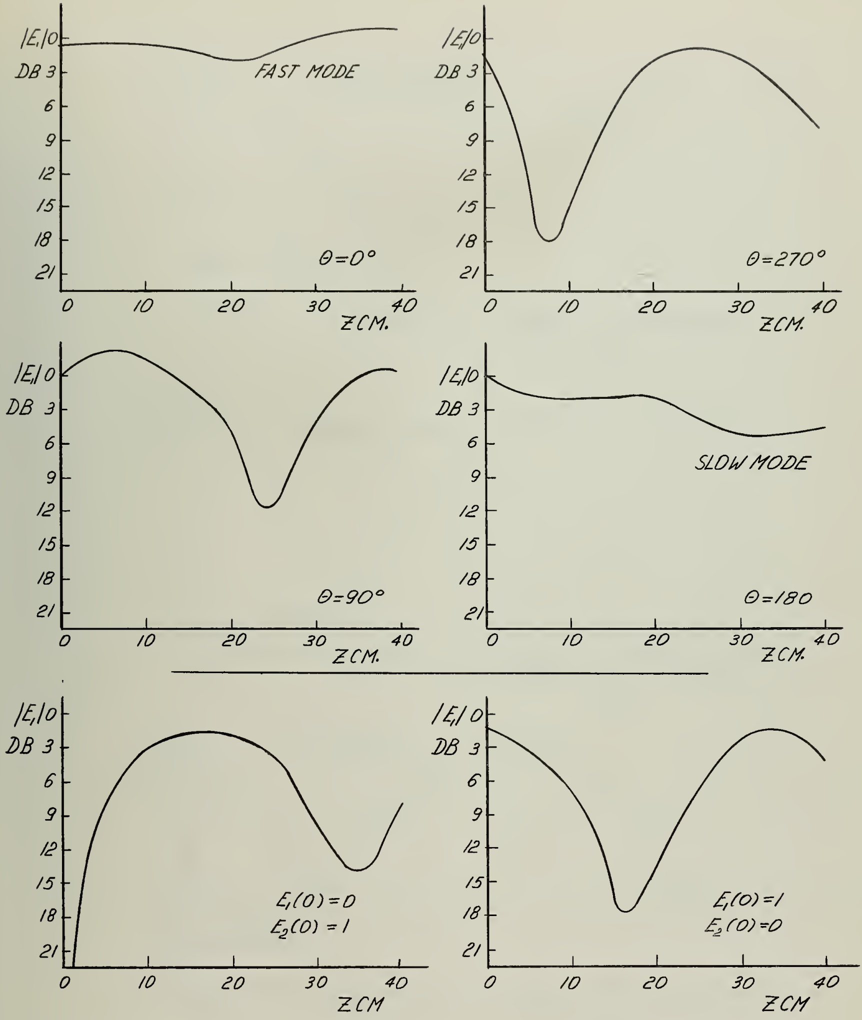

FIGURE 17 RELATIVE FIELD STRENGTH IN db VS. DISTANCE IN CM FROM START OF COUPLING. NON-RADIATING CASE, COUPLING APERTURE NO. 1, f = 11.00 kmc/sec.

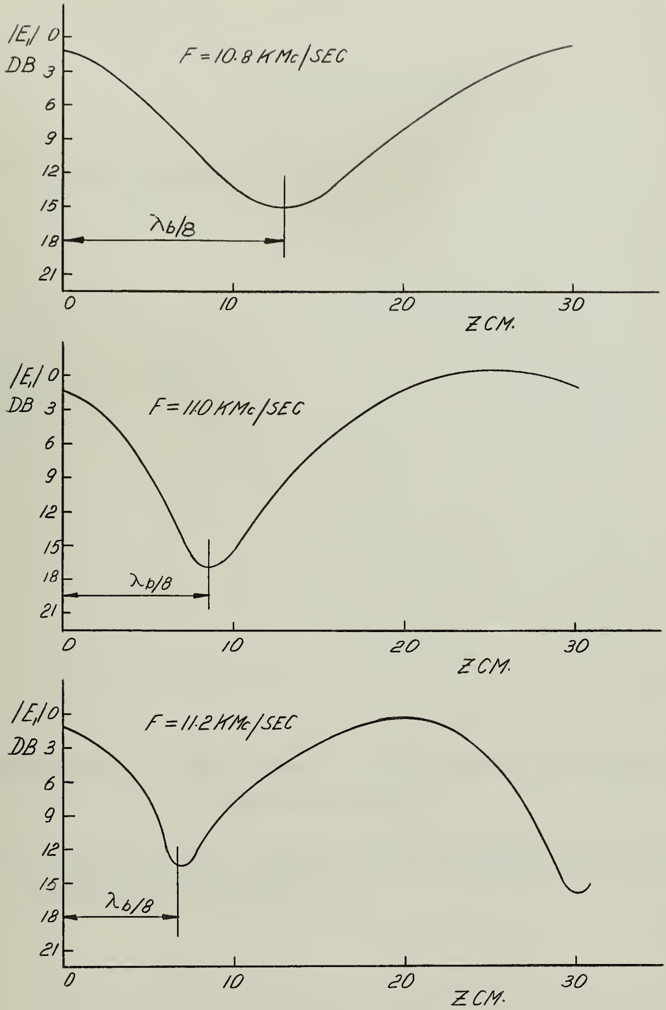

FIGURE 18 VARIATION IN BEAT WAVELENGTH AS A FUNCTION OF FREQUENCY. NON-RADIATING CASE, COUPLING APERTURE NO. 1.

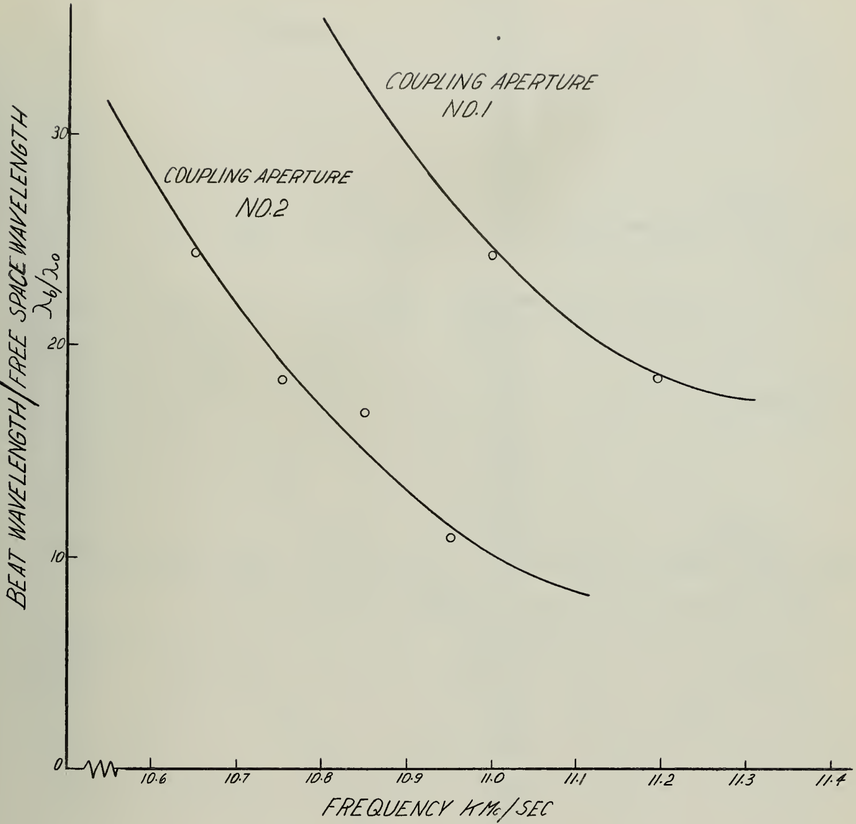

FIGURE 19 VARIATION OF BEAT WAVELENGTH WITH FREQUENCY FOR THE TWO COUPLING APERTURES, NON-RADIATING CASE.

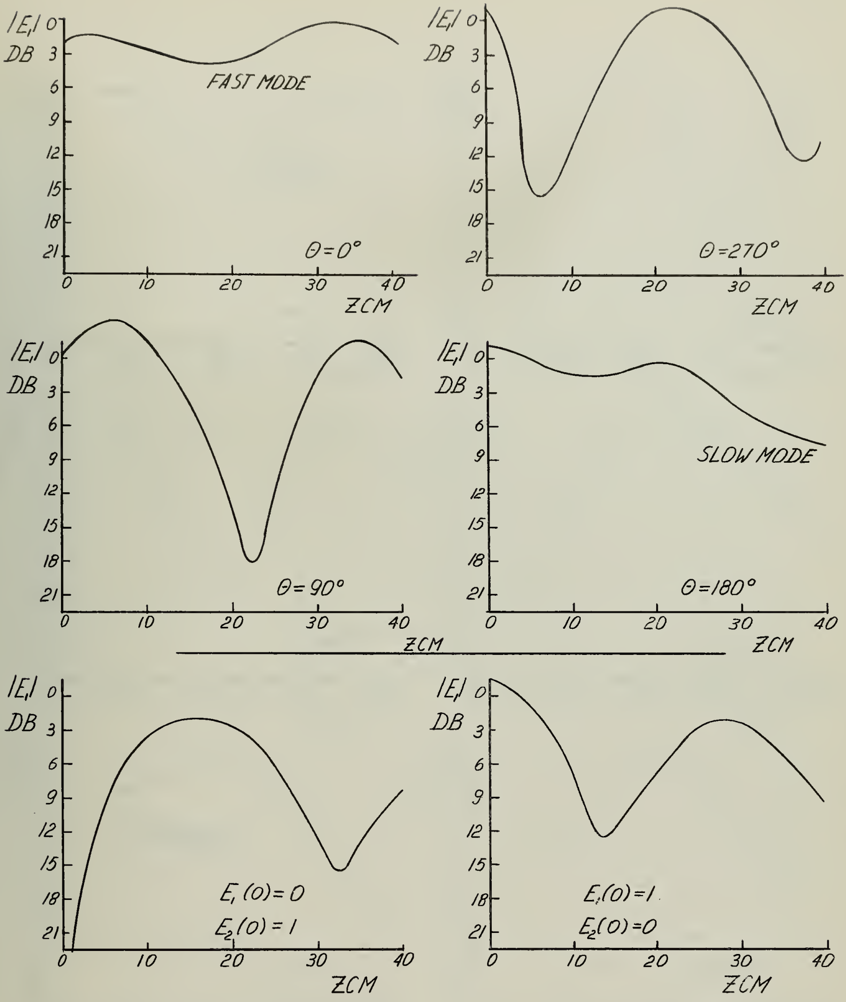

FIGURE 20 RELATIVE FIELD STRENGTH IN db VS. DISTANCE IN CM FROM START OF COUPLING. RADIATING CASE, COUPLING APERTURE NO. 1, f = 11.20 kmc/sec, RADIATING APERTURE WIDTH, 1/10 λ_o.

[illegible]

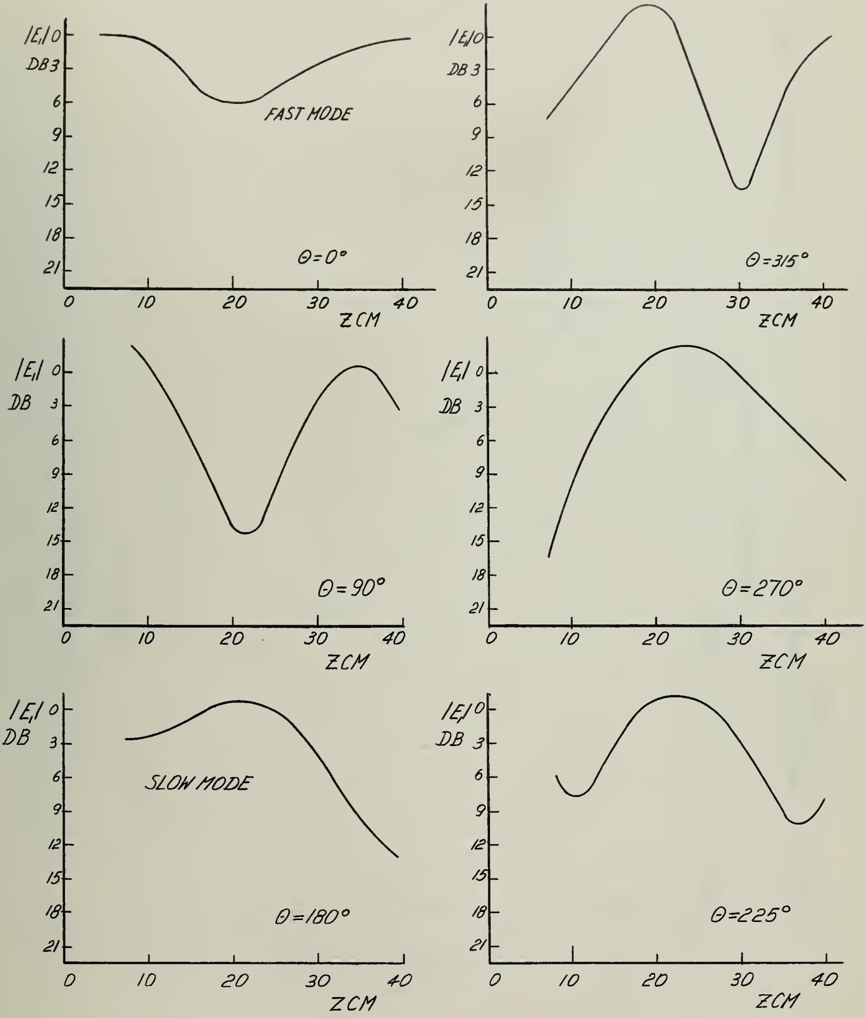

FIGURE 21 RELATIVE FIELD STRENGTH IN db VS. DISTANCE IN CM FROM START OF COUPLING, RADIATING CASE, COUPLING APERTURE NO. 1, f = 11.20 kmc/sec, RADIATING APERTURE WIDTH 1/5 λ_o.

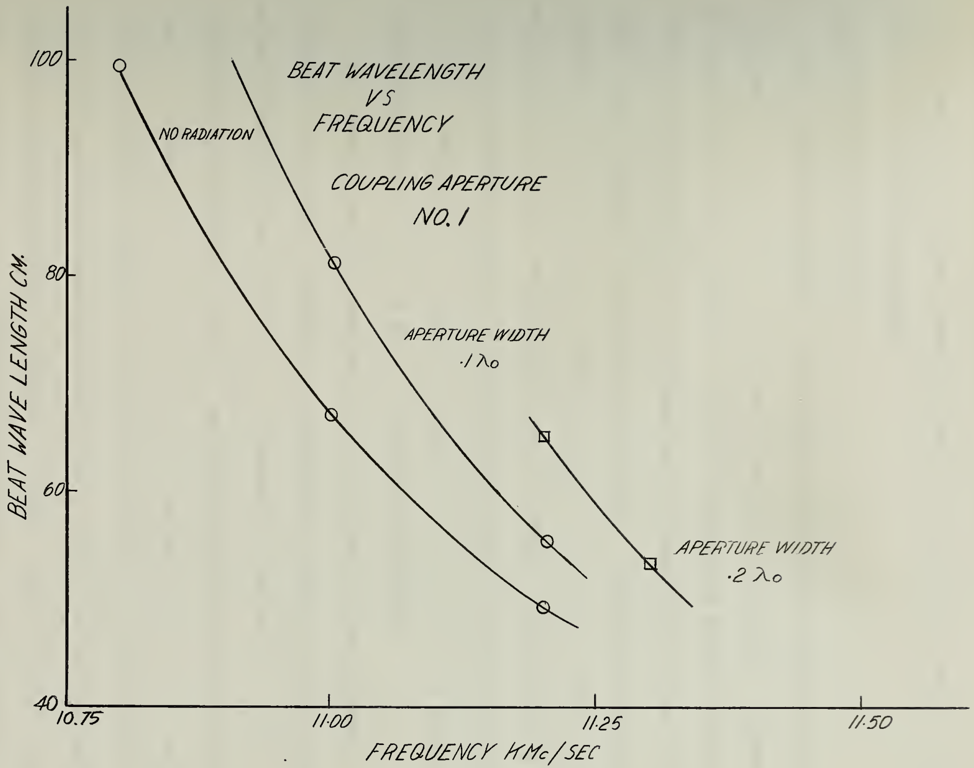

FIGURE 22 FREQUENCY VARIATION OF BEAT WAVELENGTH AND EFFECT OF RADIATION ON BEAT WAVELENGTH.

of amplitude as the wave progresses, is evident in most cases but is relatively small. At a lower frequency where the coupling is weaker the distortions are even more pronounced.

3.3 The Radiation Patterns

The radiation patterns in the plane of the ground plane were taken for the range $0^\circ \leq \phi \leq 45^\circ$ on both sides of end-fire, Figure 12. Figures 23 to 25 show these patterns together with their associated aperture distributions. The experimental curves are superposed on the theoretical curves (dotted) which were calculated in two degree increments. Equations (15) and (16) were used with $L = 11.4\ \lambda_o$, $c/v_F = .92$ and $c/v_S = 1.0$. Due to their symmetry only one half of each theoretical pattern is shown. These patterns are for the first coupling aperture at 11.20 kmc/sec with a radiating aperture width of $.2\ \lambda_o$. Note that the aperture length of $11.4\ \lambda_o$ is due to the lengthening (from the nominal $10\ \lambda_o$) of λ_b as is shown in Figure 22.

The theoretical and experimental patterns most closely agree at the extremes of the scan, although the experimental end-fire beam is smaller in amplitude by 15 per cent than its theoretical counterpart. This perhaps explains the fact that at $\Theta = 270^\circ$ the experimental main lobe is farther out than the theoretical, i.e., the fast mode component of the lobe, being greater than the slow mode component, causes the total lobe to swing farther out. Also shown is the experimental pattern for $\Theta = 90^\circ$ with its two large lobes. Symmetry of the experimental patterns on either side of end-fire is not exact. This is attributed to the mechanical imperfections of the experiment and is not a fundamental limitation; it can be corrected in practice. The antenna main lobes are roughly 20 db above the noise level of the measuring system.

A second set of radiation patterns obtained when the second coupling

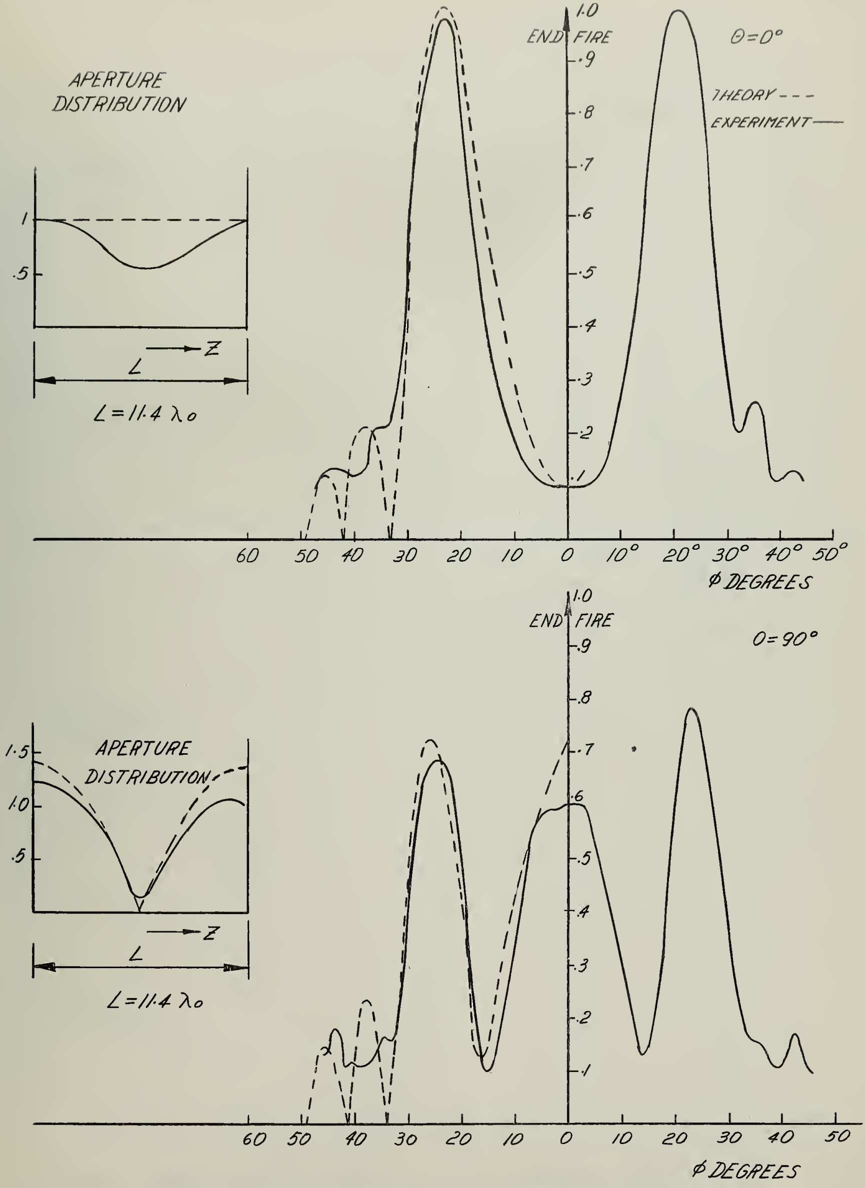

FIGURE 23 RELATIVE FIELD STRENGTH VS. φ. COUPLING APERTURE NO. 1 f = 11.20 kmc/sec. RADIATING APERTURE WIDTH, 1/5 λ_o: LENGTH, 11.4 λ_o.

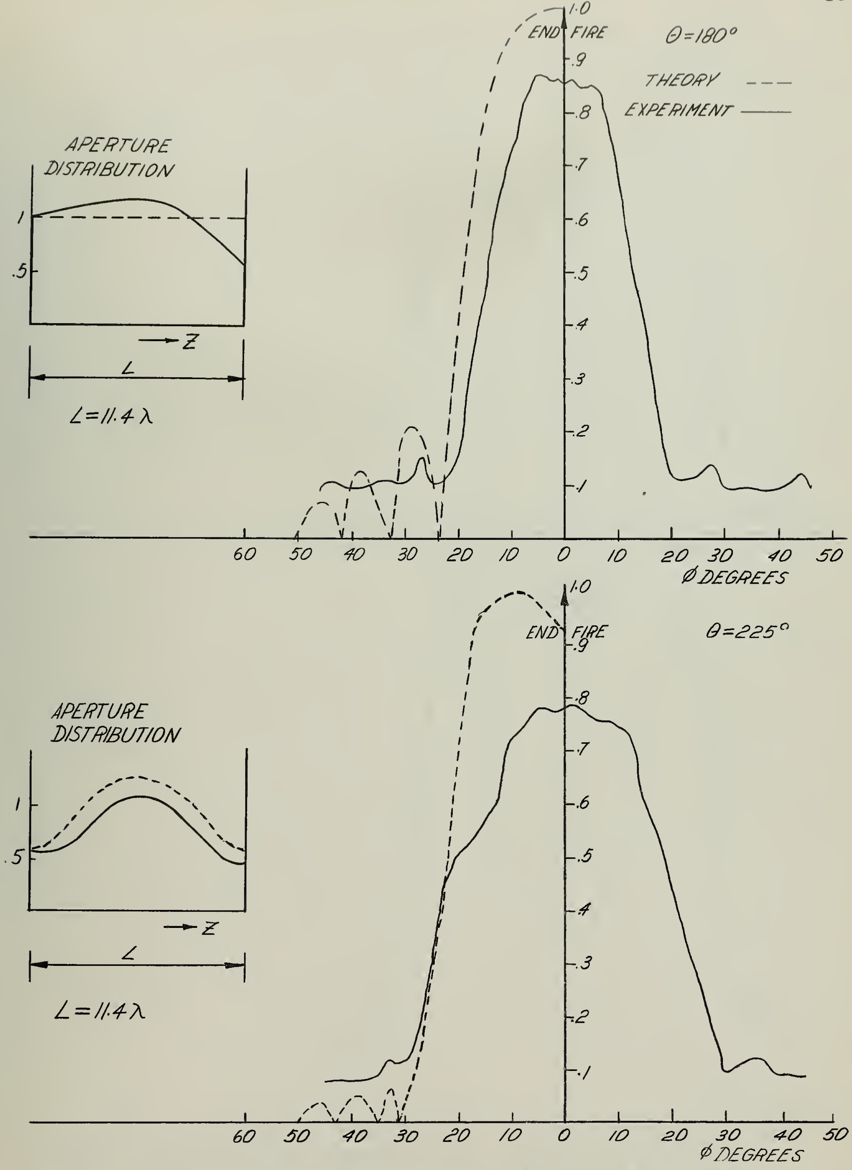

FIGURE 24 RELATIVE FIELD STRENGTH VS. ϕ. COUPLING APERTURE NO. 1, f = 11.20 kmc/sec. RADIATING APERTURE WIDTH, 1/5 λ_o: LENGTH, 11.4 λ_o.

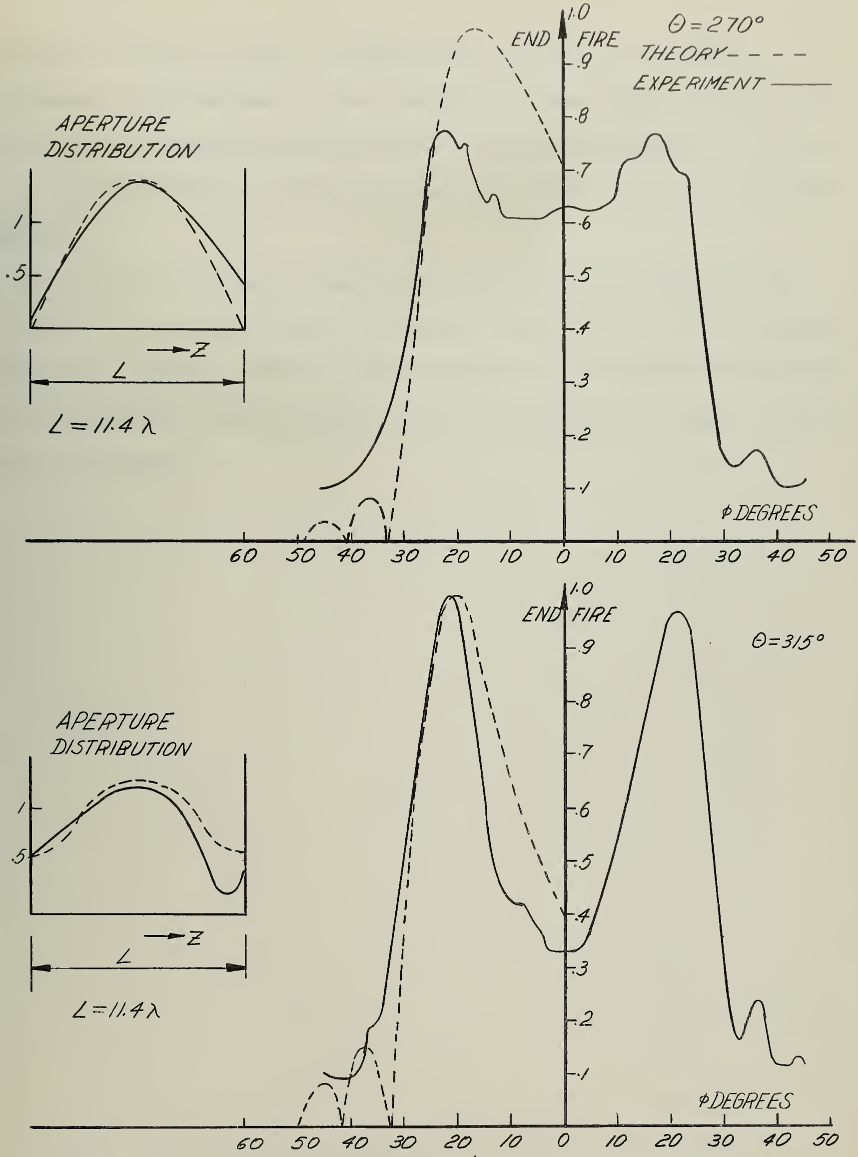

FIGURE 25 RELATIVE FIELD STRENGTH VS. ϕ. COUPLING APERTURE NO. 1 f = 11.20 kmc/sec. RADIATING APERTURE WIDTH, 1/5 λ_o: LENGTH, 11.4 λ_o.

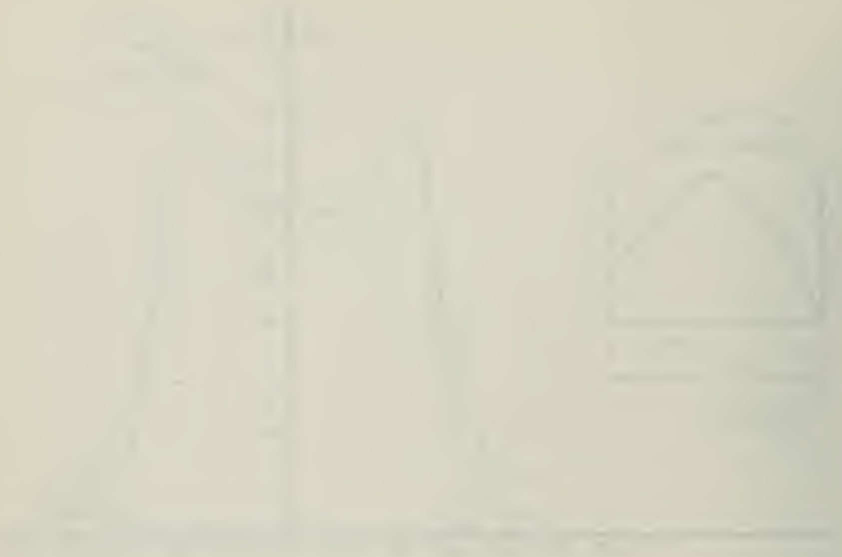

[illegible]

aperture is used are given in Figures 26 to 28. The lower operating frequency (10.85 kmc/sec), arises from the increased coupling of the larger holes of this aperture (see Figure 19). The aperture length L is 10 λ_o and its width is 3/16 inch or 0.20 λ_o. Again the theoretical curves are shown dotted.

Note that the scan is from $\phi = 12^o$ to $\phi = 30^o$. The end-fire beam ($\phi = 12^o$) is even more reduced in amplitude than that of the first coupling aperture. The scan, however, is quite smooth (if the amplitude variation is not considered). The associated aperture distributions are again distorted due to radiation.

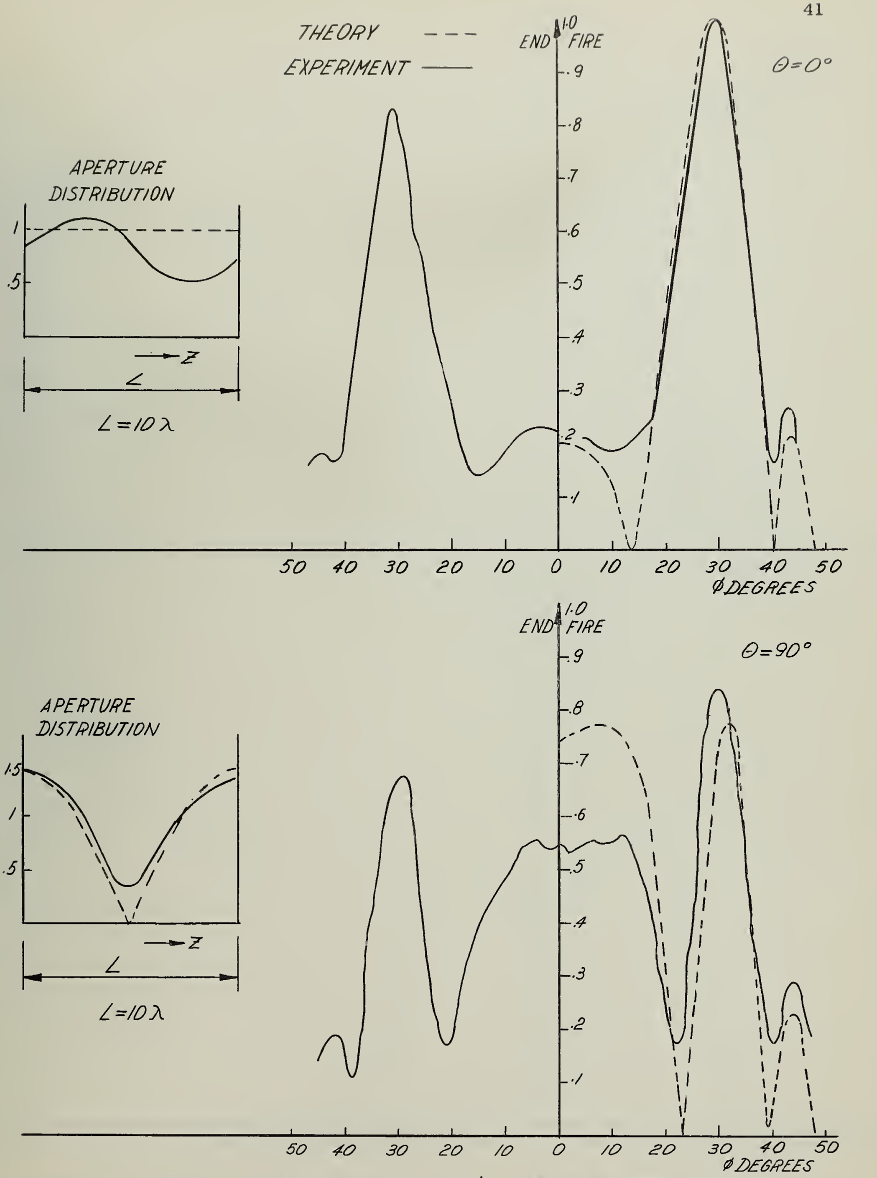

FIGURE 26 RELATIVE FIELD INTENSITY VS. ϕ. COUPLING APERTURE NO. 2
f = 10.85 kmc/sec. RADIATING APERTURE, WIDTH $1/5\lambda_o$, LENGTH, 10 λ_o

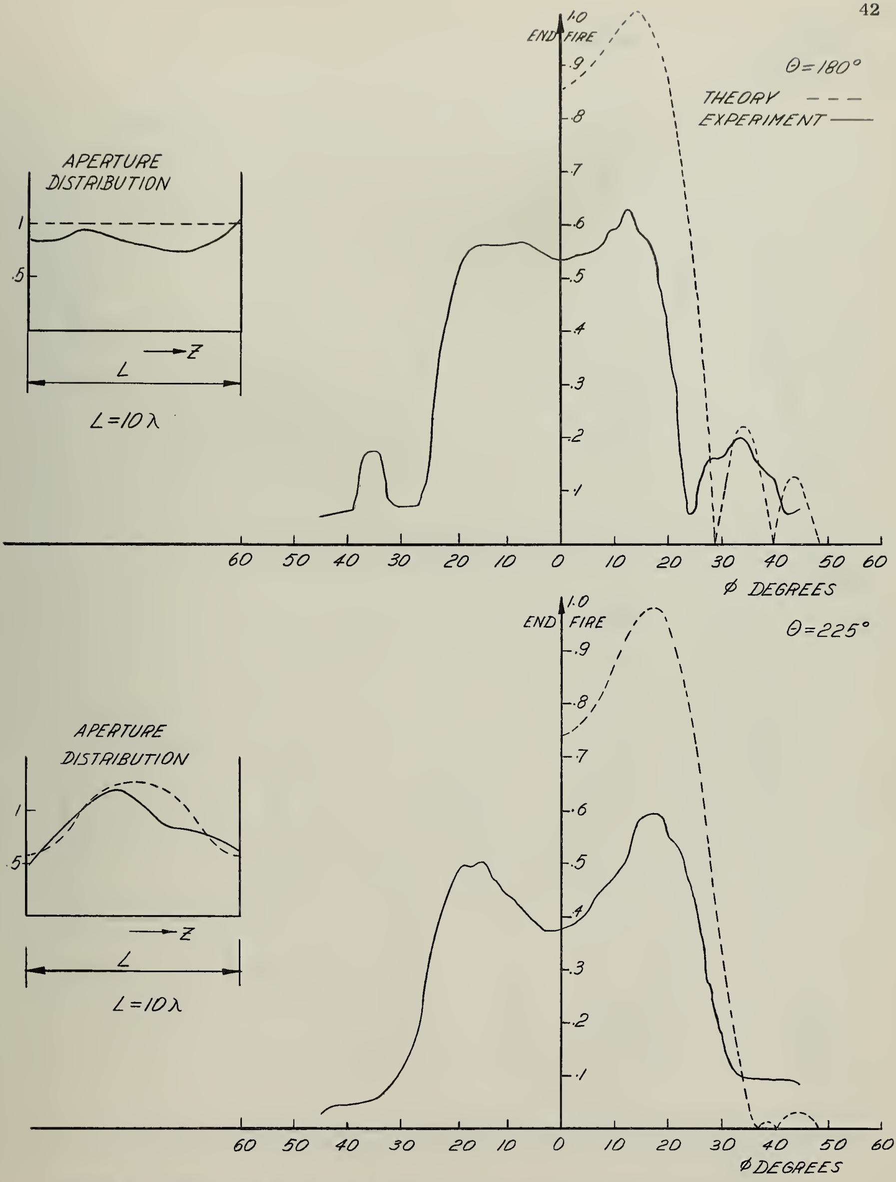

FIGURE 27 RELATIVE FIELD INTENSITY VS. ϕ. COUPLING APERTURE NO. 2
f = 10.85 kmc/sec. RADIATING APERTURE, WIDTH $1/5\lambda_0$, LENGTH, $10\lambda_0$

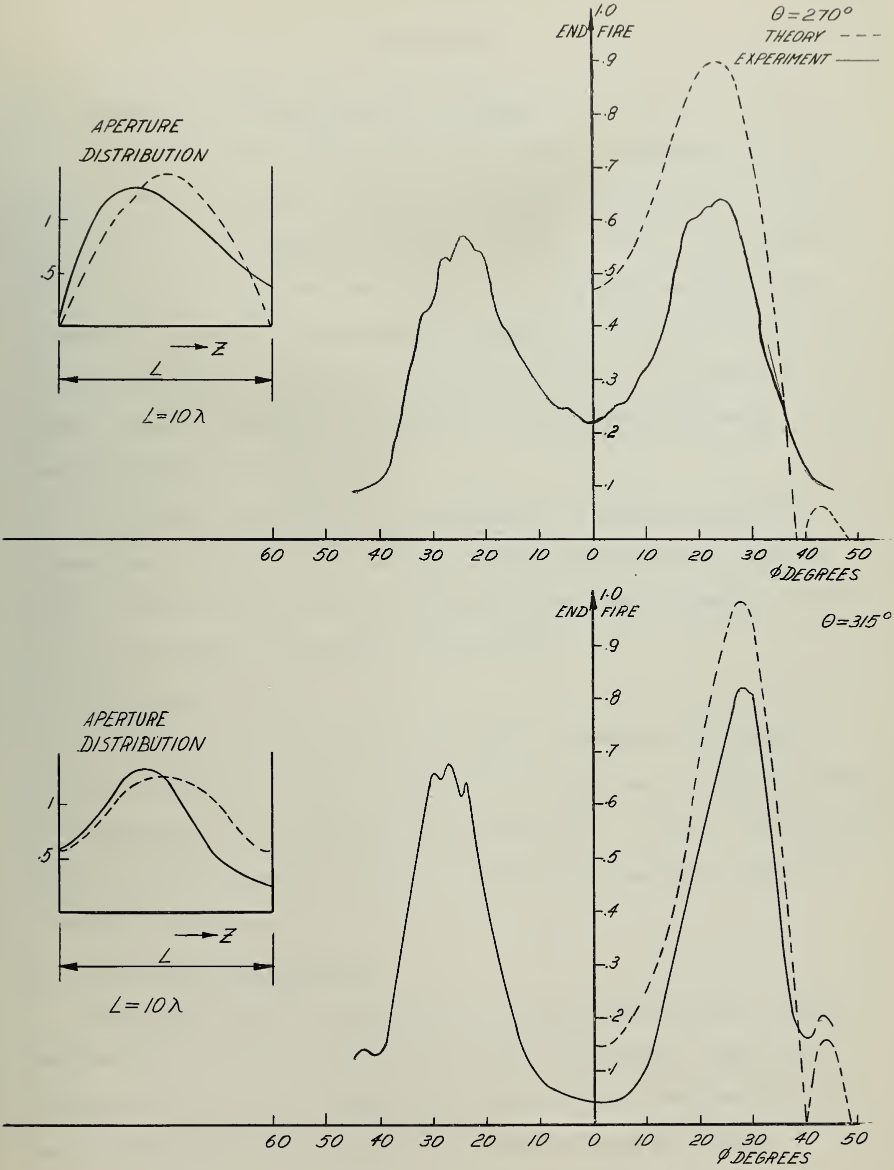

FIGURE 28 RELATIVE FIELD INTENSITY VS. ϕ. COUPLING APERTURE NO. 2
f = 10.85 kmc/sec. RADIATING APERTURE, WIDTH $1/5\lambda_o$, LENGTH, $10\lambda_o$

4. DISCUSSION

4.1 Variation in Beam Amplitude over the Scan

The slower normal mode's beam (the one closer to end-fire) is in both cases of smaller amplitude than that of the faster normal mode. A study of the variation of the standing wave ratio (Figure 11 shows the location of the slotted line) as a function of the relative phase Θ showed that the variation of power into the antenna as indicated by the SWR, was not enough to explain the large variations in the radiated field. Consequently, it appears that the radiation is different for each normal mode, being in this case greater for the faster mode.

If a constant amplitude scan is essential, it might be obtained by attenuating the signal by the necessary amount as Θ is varied. At this point it should be mentioned that both phase shift and attenuation can be done electronically, for example with ferrites.

4.2 Efficiency

As has been mentioned, the radiation must necessarily be limited in this type of antenna in order to maintain the normal modes in the waveguides. As a consequence, the efficiency is relatively poor. Further, the necessity of attenuating the signal to obtain a constant beam amplitude implies an efficiency limitation.

4.3 Other Radiating Apertures

The original paper[3] on this type of antenna suggested that a single longitudinal slot might be used as the radiating aperture. Such a slot, however, develops sharp resonances (even when it is ten wavelengths long), and its radiation pattern consequently possesses large back lobes.

An array of circular holes, approximately the same size as the coupling holes was also studied. The large back lobes due to the slot resonance were eliminated and the main lobe scanned in a predictable fashion. However, the amplitude of the main lobe tended to vary by an even greater amount than that of the second coupling aperture (Figures 26 to 28). This would require greater attenuation of the fast mode's beam in order to create a smooth scan. On the other hand, since efficiency is of secondary importance in this case, and the difficulty of manufacturing this type of aperture is less than for the slotted type, the array of circular holes is a possible alternative to the slotted aperture that has been described in this work.

4.4 Other Modes of Propagation

Hyneman[7] has shown that a surface wave can be excited by an array of closely-spaced slots. However, the geometry of the aperture used in the experimental work was such that surface waves were not excited to an important extent. Specifically, the uncoupled waveguide was allowed to radiate through the slots and the aperture field was measured. A nearly exponential decay of the field was observed. In addition the phase velocity was decreased; this was due to the loading effect of the slots themselves and has been treated theoretically by Elliott.[6] The change was apparently small enough to not affect appreciably the coupling parameters.

A measurement of the field in a longitudinal slot cut in the broad wall of the uncoupled waveguide showed a definite beat-like variation, indicating the presence of at least two modes of propagation. The large hole type of aperture was essentially free of this, showing the exponential decay of the fields due to radiation.

4.5 Frequency Sensitivity

Figure 19 shows that the frequency sensitivity of the coupling is quite extreme. It seens quite possible that, if necessary, the coupling aperture could be redesigned to give any reasonable bandwidth. As an example of this some sizes of rectangular slots used by Barkson[1] have less than one quarter of the frequency sensitivity of the apertures of Figure 19.

4.6 Radiation from Both Waveguides

It is reasonable to think that if both waveguides had identical radiating slots, they would be again identical and perhaps aperture masking would not be necessary i.e., efficiency could be greatly increased. Unfortunately the fields in the two waveguides are complementary; a null in one guide occurs at the same point as a peak in the other. Thus, if two radiating apertures were located so that they both started $\lambda_b/8$ from the start of coupling and were $\lambda_b/2$ in length, the radiation patterns would be different at all phase shift angles except two, 0^o and 180^o. At $\Theta = 90^o$ one pattern would have large side lobes while the other would be the exact opposite with small side lobes; at $\Theta = 270^o$ the situation would be reversed. Thus a symmetric scan is not possible. Two discrete beams corresponding to $\Theta = 0^o$ and $\Theta = 180^o$ are, however.

Staggering the aperture locations so that each aperture distribution is properly tapered might give some useful results.

Finally, if some resistance material is located in the bottom waveguide, it could simulate radiation loss and make the two waveguides again identical electrically. An efficiency of fifty per cent could be approached.

5. CONCLUSIONS

A flush-mounted antenna of the traveling wave type has been shown to give a fairly smooth scan through an angle of about twenty degrees from the end fire direction. Smaller scans of any size or location (in the forward quadrant) with correspondingly smaller beamwidths are also possible. The only limitation is that the beamwidth must be approximately equal to the scan itself. The antenna is not efficient but its design is relatively simple, in that its operation depends on only one phase shifter. The radiating aperture of a single longitudinal slot is unsatisfactory because of resonance and the array of closely spaced transverse slots is preferable to a number of large circular holes.

REFERENCES

1. Barkson, J. A., "Coupling of Rectangular Waveguides Having a Common Broad Wall Which Contains Uniform Transverse Slots," Ph. D. Thesis, University of Illinois, 1957. (Also available as a technical report, Hughes Aircraft Company.)

2. Morse, P. M., Vibration and Sound McGraw-Hill, 1948, p. 53.

3. Weeks, W. L., "Coupled Waveguide Excitation of Traveling Wave Slot Antennas," University of Illinois, Antenna Laboratory Technical Report No. 27, Dec. 1957.

4. Weeks, W. L., "Phase Velocities in Rectangular Waveguide Partially Filled with Dielectric," University of Illinois Antenna Laboratory Technical Report No. 28, Dec. 1957.

5. Stegen, R. J. and Reed, R. H., "Arrays of Closely-Spaced Non-Resonant Slots," I.R.E. Trans. Vol. AP-2, July 1954, pp. 109-112.

6. Elliot, R. S. and Kelly, K. C., "Serrated Waveguide," I.R.E. Trans. Vol. AP-5, July 1957, pp. 270-283.

7. Hyneman, Richard F., "Closely Spaced Transverse Slots in Rectangular Waveguide," University of Illinois Antenna Laboratory Technical Report No. 14, Dec. 1956.

8. Jordan, E. C., Electromagnetic Waves and Radiating Systems, Prentice-Hall, 1950, p. 252.

APPENDIX A

PHASE VELOCITY VARIATION WITH DISTANCE ALONG THE WAVEGUIDE

Although the normal mode phase velocities in the waveguide are constant, it can be shown that the phase velocity of the total field in the waveguide is in general a function of distance along the waveguide as well as of the relative phase angle Θ.

This can be most easily shown by considering the phase velocity gradient. Consider the expression (Equation 10 of Part I) for the line voltage.

$$V_1 = e^{j\frac{\Theta}{2}} \left[\cos\frac{\Theta}{2}\, e^{-j\beta_F z} + j \sin\frac{\Theta}{2}\, e^{-j\beta_S z} \right] \tag{A.1}$$

which can be rewritten as

$$\begin{aligned} V_1 &= e^{j(\frac{\Theta}{2} - \beta_a z)} \cos\frac{\Theta}{2} \left[e^{j\beta_b z} + j \tan\frac{\Theta}{2}\, e^{-j\beta_b z} \right] \\ V_1 &= \cos\frac{\Theta}{2}\, M(\Theta, \beta_b z)\, e^{j(\frac{\Theta}{2} - \beta_a Z + \varphi(\Theta, \beta_b z))} \end{aligned} \tag{A.2}$$

Its argument is

$$\frac{\Theta}{2} - \beta_a z + \varphi(\Theta, \beta_b z)$$

or

$$\operatorname{Arg} V_1 = \frac{\Theta}{2} - \beta_a Z + \operatorname{Im}\left[\ell n \left\{ e^{j\beta_b z} + j \tan\frac{\Theta}{2}\, e^{-j\beta_b z} \right\} \right]$$

Now if the phase constant is not a function of z, the derivative of Arg V_1

[illegible]

[illegible]

[illegible]

$$[illegible]$$

[illegible]

$$[illegible]$$

$$[illegible]$$

[illegible]

$$[illegible]$$

$$[illegible]$$

[illegible]

should be constant.

$$\frac{d \text{ Arg } V_1}{dz} = -\beta_a + \beta_b R_e \left[\frac{1 - j \tan \frac{\theta}{2} e^{-j2\beta_b z}}{1 + j \tan \frac{\theta}{2} e^{-j2\beta_b z}} \right] \tag{A.3}$$

The coefficient of β_b is of the same form as the expression for the input resistance of a transmission line z units long and with a termination whose reflection coefficient is $-j \tan \theta/2$ [8]. If a Smith chart is used one sees that as z increases the "reflection coefficient vector" spins about the origin and in general does not coincide with any contour of constant resistance. Thus the effective phase constant is a function of z as well as of θ.

At $\theta = 0^\circ$, however, the "reflection coefficient" is zero and for all z the input resistance (normalized) is unity; the effective phase constant is $-(-\beta_a + \beta_b)$ or β_F. At $\theta = 90^\circ$ or 270° the "reflection coefficient" has unit magnitude and its vector coincides with the zero resistance contour; the phase constant now is β_a for all z. At $\theta = 180^\circ$, however, the analogy breaks down somewhat in that the reflection coefficient amplitude is infinite, an impossibility for passive loads. However, inspection of Equation (A.3) shows that for this relative phase setting the phase constant is β_S for all z.

It is interesting to note that far from being a well behaved function, the effective phase constant is singular at some values of θ and z. This occurs when

$$1 + j \tan \frac{\theta}{2} e^{-j2\beta_b z} = 0$$

(see Equation (A.3).

The respective values of Θ and $\beta_b z$ are $\Theta = 90^\circ$ or 270°, and

$$\beta_b z = \frac{3\pi}{4} + n\pi \qquad \text{or} \qquad \frac{\pi}{4} + n\pi \, , \qquad n = 0,\ 1,\ 2,\ 3,\ \ldots$$

It follows that at these points the phase velocity $(\frac{\omega}{\beta})$ is zero.

APPENDIX B

ANALYSIS FOR THE CASE OF LOSS IN ONE OF THE TRANSMISSION LINES

Let there be a shunt conductance per unit length δ inserted in line 1. Then the various circuit parameters are as follows:*

$$jZ_{11} = jZ_{22}, \; jY_{11} = jY_{22} + \delta, \; jZ_{12} = jZ_{21}, \; jY_{12} = jY_{21}.$$

and

$$\gamma_1^{\,2} = -(Z_{22}Y_{22} + Z_{12}Y_{21}) + jZ_{11}\delta$$

$$\gamma_2^{\,2} = -(Z_{22}Y_{22} + Z_{12}Y_{21}) = \gamma_1^{\,2} - jZ_{11}\delta$$

$$\gamma_1^{\,2} - \gamma_2^{\,2} = jZ_{11}\delta$$

$$c^2_{12} = -(Z_{12}Y_{22} + Z_{11}Y_{12}), \; c^2_{21} = -(Z_{12}Y_{22} + Y_{12}Z_{11}) + jZ_{12}\delta = c^2_{12} + jZ_{12}\delta.$$

Now

$$\gamma_{\substack{F\\S}}^{\,2} = \frac{\gamma_1^{\,2} + \gamma_2^{\,2}}{2} \mp \frac{1}{2}\sqrt{(\gamma_1^{\,2} - \gamma_2^{\,2})^2 + 4c^2_{12}\,c^2_{21}}$$

$$= \gamma_2^{\,2} + j\frac{Z_{11}\delta}{2} \mp \frac{1}{2}\sqrt{-Z^2_{11}\delta^2 + 4c^4_{12} + 4jc^2_{12}Z_{12}\delta}$$

$$= \gamma_2^{\,2} + j\frac{Z_{11}\delta}{2} \mp \sqrt{c^4_{12} - \frac{Z^2_{11}\delta^2}{4} + j\,c^{\,2}_{12}Z_{12}\delta}$$

and if δ is sufficiently small the surd simplifies to

$$c^2_{12} - \frac{Z_{11}^{\,2}\delta^2}{8c^{\,2}_{12}} + j\frac{Z_{12}\delta}{2}$$

---

* Z_{11}, Z_{22}, Y_{11}, δ etc. are real numbers.

Hence

$$\gamma_{\substack{F\\S}}^{2} \simeq (\gamma_2^{2} + j\,\frac{Z_{11}\delta}{2}) \mp (c_{12}^{2} - \frac{Z_{11}^{2}\delta^{2}}{8\,c_{12}^{2}} + j\,\frac{Z_{12}\delta}{2})$$

Separating into real and imaginary parts gives

$$\gamma_{\substack{F\\S}}^{2} \simeq \gamma_2^{2} \mp (c_{12}^{2} - \frac{Z_{11}^{2}\delta^{2}}{8\,c_{12}^{2}}) + j\left[\frac{Z_{11}\delta}{2} \mp \frac{Z_{12}\delta}{2}\right]$$

and since c_{12}^2 and δ are both small, one can write

$$\gamma_F = j\left\{|\gamma_2| - \frac{1}{2}\left[\left|\frac{c_{12}^{2}}{\gamma_2}\right| - \left|\frac{Z_{11}^{2}\delta^{2}}{8\gamma_2 c_{12}^{2}}\right|\right]\right\} + \frac{\delta}{4|\gamma_2|}(Z_{11} - Z_{12})$$

$$= j\left\{\beta_a - \beta_b'\right\} + \alpha_F$$

$$\gamma_S = j\left\{|\gamma_2| + \frac{1}{2}\left[\left|\frac{c_{12}}{\gamma_2}\right| - \left|\frac{Z_{11}^{2}\delta^{2}}{8\gamma_2 c_{12}^{2}}\right|\right]\right\} + \frac{\delta}{4|\gamma_2|}(Z_{11} + Z_{12})$$

$$= j\left\{\beta_a + \beta_b'\right\} + \alpha_S$$

Note that the resulting β_b' is less than for the lossless case. This means that λ_b is greater and is evident in the experimental work, (see Figure 22). The attenuation of the slow mode is larger than that of the fast mode. However, it can be shown that for weak coupling $Z_{11} \gg Z_{12}$, and so the two attenuation constants are practically the same.

ANTENNA LABORATORY
TECHNICAL REPORTS AND MEMORANDA ISSUED

Contract AF33(616)-310

"Synthesis of Aperture Antennas," Technical Report No. 1, C.T.A. Johnk October, 1954.

"A Synthesis Method for Broad-band Antenna Impedance Matching Networks," Technical Report No. 2, Nicholas Yaru, 1 February 1955.

"The Asymmetrically Excited Spherical Antenna," Technical Report No. 3, Robert C. Hansen, 30 April 1955.

"Analysis of an Airborne Homing System," Technical Report No. 4, Paul E. Mayes, 1 June 1955, (CONFIDENTIAL).

"Coupling of Antenna Elements to a Circular Surface Waveguide," Technical Report No. 5, H. E. King and R. H. DuHamel, 30 June 1955.

"Input Impedance of a Spherical Ferrite Antenna wigh a Latitudinal Current," Technical Report No. 6, W. L. Weeks, 20 August 1955.

"Axially Excited Surface Wave Antennas," Technical Report No. 7, D. E. Royal, 10 October 1955.

"Homing Antennas for the F-86F Aircraft (450-2500mc)," Technical Report No. 8 P. E. Mayes, R. F. Hyneman, and R. C. Becker, 20 February 1957. (CONFIDENTIAL)

"Ground Screen Pattern Range," Technical Memorandum No. 1, Roger R. Trapp, 10 July 1955.

Contract AF33(616)-3220

"Effective Permeability of Spheroidal Shells," Technical Report No. 9, E. J. Scott and R. H. DuHamel, 16 April 1956.

"An Analytical Study of Spaced Loop ADF Antenna Systems," Technical Report No. 10, D. G. Berry and J. B. Kreer, 10 May 1956.

"A Technique for Controlling the Radiation from Dielectric Rod Wavequides," Technical Report No. 11, J. W. Duncan and R. H. DuHamel, 15 July 1956.

"Directional Characteristics of a U-Shaped Slot Antenna," Technical Report No. 12, Richard C. Becker, 30 September 1956.

"Impedance of Ferrite Loop Antennas," Technical Report No. 13, V. H. Rumsey and W. L. Weeks, 15 October 1956.

"Closely Spaced Transverse Slots in Rectangular Waveguide " Technical Report No. 14, Richard F. Hyneman, 20 December 1956.

"Distributed Coupling to Surface Wave Antennas," Technical Report No. 15, Ralph Richard Hodges, Jr., 5 January 1957.

"The Characteristic Impedance of the Fin Antenna of Infinite Length," Technical Report No. 16, Robert L. Carrel, 15 January 1957.

"On the Estimation of Ferrite Loop Antenna Impedance," Technical Report No. 17, Walter L. Weeks, 10 April 1957.

"A Note Concerning a Mechanical Scanning System for a Flush Mounted Line Source Antenna," Technical Report No. 18, Walter L. Weeks, 20 April 1957.

"Broadband Logarithmically Periodic Antenna Structures," Technical Report No. 19, R. H. DuHamel and D. E. Isbell, 1 May 1957.

"Frequency Independent Antennas," Technical Report No. 20, V. H. Rumsey, 25 October 1957.

"The Equiangular Spiral Antenna," Technical Report No. 21, J. D. Dyson, 15 September 1957.

"Experimental Investigation of the Conical Spiral Antenna," Technical Report No. 22, R. L. Carrel, 25 May 1957.

"Coupling Between a Parallel Plate Waveguide and a Surface Waveguide," Technical Report No. 23, E.J. Scott, 10 August 1957.

"Launching Efficiency of Wires and Slots for a Dielectric Rod Waveguide," Technical Report No. 24, J.W. Duncan and R.H. DuHamel, August 1957.

"The Characteristic Impedance of an Infinite Biconical Antenna of Arbitrary Cross Section," Technical Report No. 25, Robert L. Carrel, August 1957.

"Cavity-Backed Slot Antennas," Technical Report No. 26, R.J. Tector, 30 October 1957.

"Coupled Waveguide Excitation of Traveling Wave Slot Antennas," Technical Report No. 27, W.L. Weeks, 1 December 1957.

"Phase Velocities in Rectangular Waveguide Partially Filled with Dielectric," Technical Report No. 28, W.L. Weeks, 20 December 1957.

"Measuring the Capacitance per Unit Length of Biconical Structures of Arbitrary Cross Section," Technical Report No. 29, J.D. Dyson, 10 January 1958.

"Non-Planar Logarithmically Periodic Antenna Structure," Technical Report No. 30, D.W. Isbell, 20 February 1958.

"Electromagnetic Fields in Rectangular Slots," Technical Report No. 31, N.J. Kuhn and P.E. Mast, 10 March 1958.

"The Efficiency of Excitation of a Surface Wave on a Dielectric Cylinder," Technical Report No. 32, J.W. Duncan, 25 May 1958.

"A Unidirectional Equiangular Spiral Antenna," Technical Report No. 33, J.D. Dyson, 10 July 1958.

"Dielectric Coated Spheroidal Radiators," Technical Report No. 34, W.L. Weeks, 12 September 1958.

"A Theoretical Study of the Equiangular Spiral Antenna," Technical Report No. 35, P.E. Mast, 12 September 1958.

Contract AF33(616)-6079

"Use of Coupled Waveguides in a Traveling Wave Scanning Antenna," Technical Report No. 36, R.H. MacPhie, 30 April 1959.

DISTRIBUTION LIST

One copy each unless otherwise indicated

Armed Services Technical Information Agency
Arlington Hall Station
Arlington 12, Virginia
3 copies, 1 repro.

Commander
Wright Air Development Center
Wright-Patterson Air Force Base, Ohio
ATTN: WCLRS-6, Mr. F.E. Burnham
3 copies

Commander
Wright Air Development Center
ATTN: WCLNQ-4, Mr. M. Draganjac
Wright-Patterson Air Force Base, Ohio

Commander
Wright Air Development Center
ATTN: WCOSI, Library
Wright-Patterson Air Force Base, Ohio

Director
Evans Signal Laboratory
ATTN: Technical Document Center
Belmar, New Jersey

Commander
U.S. Naval Air Test Center
ATTN: ET-315, Antenna Section
Patuxent River, Maryland

Chief
Bureau of Ordnance
Department of the Navy
ATTN: Mr. C.H. Jackson, Code Re 9a
Washington 25, D. C.

Commander
Hq. A. F. Cambridge Research Center
Air Research and Development Command
Laurence G. Hanscom Field
ATTN: CRRD, R. E. Hiatt
Bedford, Massachusetts

Commander
Air Force Missile Test Center
Patrick Air Force Base, Florida
ATTN: Technical Library

Director
Ballistics Research Laboratory
ATTN: Ballistics Measurement Lab.
Aberdeen Proving Ground, Maryland

Office of the Chief Signal Officer
ATTN: SIGNET-5
Eng. & Technical Division
Washington 25, D. C.

Commander
Rome Air Development Center
ATTN: RCERA-1 D. Mather
Griffiss Air Force Base
Rome, New YOrk

Airborne Instruments Lab., Inc.
ATTN: Dr. E. G. Fubini
Antenna Section
160 Old Country Road
Mineola, New York
M/F Contract AF33(616)-2143

Andrew Alford Consulting Engineers
ATTN: Dr. A. Alford
299 Atlantic Avenue
Boston 10, Massachusetts
M/F Contract AF33(038)-23700

Bell Aircraft Corporation
ATTN: Mr. J. D. Shantz
Buffalo 5, New York
M/F Contract W-33(038)-14169

Chief
Bureau of Ships
Department of the Navy
ATTN: Code 838D, L. E. Shoemaker
Washington 25, D.C.

DISTRIBUTION LIST (CONTINUED)

McDonnell Aircraft Corporation
ATTN: Engineering Library
M/F Contract AF33(600)-8743
Lambert Municipal Airport
St. Louis 21, Missouri

Dr. L. Cutrona
University of Michigan
Aeronautical Research Center
M/F Contract AF33(038)-21573
Willow Run Airport
Ypsilanti, Michigan

Professor H. J. Zimmermann
Research Lab. of Electronics
Massachusetts Institute of Technology
M/F Contract AF33(616)-2107
Cambridge, Massachusetts

Dr. J. A. Marsh
North American Aviation, Inc.
Aerophysics Laboratory
M/F Contract AF33(038)18319
12214 Lakewood Boulevard
Downey, California

Mr. Dave Mason
Engineering Data Section
North American Aviation, Inc.
M/F Contract AF33(038)18319
Los Angeles International Airport
Los Angeles 45, California

Northrop Aircraft, Incorporated
ATTN: Northrop Library
Dept. 2135
M/F Contract AF33(600)-22313
Hawthorne, California

Radioplane Company
M/F Contract AF33(600)-23893
Van Nuys, California

Lockheed Aircraft Corporation
ATTN: C. L. Johnson
P.O. Box 55
M/F NOa(s)-52-763
Burbank, California

Robert Borts
Raytheon Manufacturing Company
Wayland Laboratory, Wayland, Mass.

Republic Aviation Corporation
ATTN: Engineering Library
M/F Contract AF33(038)-14810
Farmingdale
Long Island, New York

Sperry Gyroscope Company
ATTN: Mr. B. Berkowitz
M/F Contract AF33(038)-14524
Great Neck
Long Island, New York

Mr. George Cramer
Temco Aircraft Cprporation
Contract AF33(600)21714
Garland, Texas

George Giffin
Farnsworth Electronics Co.
Marked For Con. AF33(600)-25523
Ft. Wayne, Indiana

Mr. James D. Leonard
North American Aviation, Inc.
Contract NOa(s) 54-323
4300 E. Fifth Avenue
Columbus, Ohio

Mr. P. D. Newhouser
Development Engineering
Westinghouse Electric Corporation
Air Arm Division
Contract AF33(600)-27852
Friendship Airport, Maryland

Air Force Development Field
Representative
ATTN: Capt. Carl B. Ausfahl
Code 1010
Naval Research Laboratory
Washington 25, D.C.

Chief of Naval Research
Department of the Navy
ATTN: Mr. Harry Harrison
Code 427
Room 2604, Bldg. T-3
Washington 25, D.C.

DISTRIBUTION LIST (CONTINUED)

Sylvania Electric Products, Inc.
Electronic Defense Laboratory
M/F Contract DA 36-039-sc-75012
P.O. Box 205
Mountain View, California

Stanford Electronics Laboratory
Stanford University
ATTN: Applied Electronics Lab.
Document Library
Stanford, California

Radio Corporation of America
R.C.A. Laboratories Division
Princeton, New Jersey

Electrical Engineering Res. Lab.
University of Texas
Box 8026, University Station
Austin, Texas

Dr. Robert Hansen
8356 Chase Avenue
Los Angeles 45, California

Technical Library
Bell Telephone Laboratories
463 West Street
New York 14, New York

Dr. R. E. Beam
Microwave Laboratory
Northwestern University
Evanston, Illinois

Dr. H. G. Booker
Department of Electrical Engineering
Cornell University
Ithaca, New York

Applied Physics Laboratory
Johns Hopkins University
8621 Georgia Avenue
Silver Spring, Maryland

Exchange and Gift Division
The Library of Congress
Washington 25, D.C.

Ennis Kuhlman
% McDonnell Aircraft
P.O. Box 516
Lambert Municipal Airport
St. Louis 21, Missouri

Mr. Roger Battie
Supervisor, Technical Liaison
Sylvania Electric Products, Inc.
Electronic Systems Division
P.O. Box 188
Mountain View, California

Physical Science Lab.
ATTN: R. Dressel
New Mexico College of A and MA
State College, New Mexico

Mrs. E. L. Hufschmidt, Librarian
Technical Reports Collection
303 A. Pierce Hall
Harvard University
Cambridge 38, Massachusetts

Dr. R. H. DuHamel
Collins Radio Company
Cedar Rapids, Iowa

Dr. R. F. Hyneman
5116 Marburn Avenue
Los Angeles 43, California

Director
Air University Library
ATTN: AUL-8489
Maxwell AFB, Alabama

Mary Lou Fields, Acquisitions
Stanford Research Institute
Documents Center
Menlo Park, California

Dr. Harry Letaw, Jr.
Research Division
Raytheon Manufacturing Co.
Waltham 54, Massachusetts

Canoga Corporation
5955 Sepulveda Boulevard
M/F Contract AF08(603)-4327
P.O. Box 550
Van Nuys, California

DISTRIBUTION LIST (CONTINUED)

Director
Naval Research Laboratory
ATTN: Dr. J. I. Bohnert
Anacostia
Washington 25, D.C.

National Bureau of Standards
Department of Commerce
ATTN: Dr. A. G. McNish
Washington 25, D.C.

Director
U.S. Navy Electronics Lab
Point Loma
San Diego 52, California

Commander
USA White Sands Signal Agency
White Sands Proving Command
ATTN: SIGWS-FC-02
White Sands, New Mexico

Consolidated Vultee Aircraft Corp
Fort Worth Division
ATTN: C. R. Curnutt
M/F Contract AF33(038)-21117
Fort Worth, Texas

Dorne & Margolin
29 New York Ave.
M/F Contract AF33(616)-2037
Westbury
Long Island, New York

Douglas Aircraft Company, Inc.
ATTN: J. C. Buckwalter
M/F Contract AF33(600)-25669
Long Beach Plant
Long Beach 1, California

Boeing Airplane Company
ATTN: F. Bushman
M/F Contract AF33(038)-31096
7755 Marginal Way
Seattle, Washington

Chance-Vought Aircraft Division
United Aircraft Corporation
ATTN: Mr. F. N. Kickerman
THRU: BuAer Representative
Dallas, Texas

Consolidated-Vultee Aircraft Corp.
ATTN: Mr. R. E. Honer
M/F Contract AF33(600)-26530
P.O. Box 1950
San Diego 12, California

Grumann Aircraft Engineering Corp.
ATTN: J.S. Erickson,
Asst. Chief, Avionics Dept.
M/F Contract NOa(s) 51-118
Bethpage
Long Island, New York

Hallicrafters Corporation
ATTN: Norman Foot
M/F Contract AF33(600)-26117
440 W. 5th Avenue
Chicago, Illinois

J. D. Funderburg,
Counter Measures Section
Hoffman Laboratories
Los Angeles, California
M/F Contract AF33(604)-17231

D. Adcock
Hughes Aircraft Corporation
Division of Hughes Tool Company
M/F Contract AF33(600)-27615
Florence Avenue at Teale
Culver City, California

Dr. E. C. Jordan
University of Illinois
Head, Department of Electrical Eng.
Urbana, Illinois

Johns Hopkins University
Radiation Laboratory
ATTN: Librarian
M/F Contract AF33(616)-68
1315 St. Paul Street
Baltimore 2, Maryland

Glen L. Martin Company
M/F Contract AF33(600)-21703
Baltimore 3, Maryland

DISTRIBUTION LIST (CONTINUED)

Beech Airctaft Corporation
ATTN: Chief Engineer
M/F Contract AF33(600)-20910
6600 E. Central Avenue
Wichita 1, Kansas

Land-Air, Incorporated
Cheyenne Division
ATTN: Mr. R. J. Klessig
Chief Engineer
M/F Contract AF33(600)-22964
Cheyenne, Wyoming

Director, National Security Agency
RADE 1GM, ATTN: Lt. Manning
Washington 25, D.C.

K. S. Kelleher
Melpar, Inc.
3000 Arlington Blvd.
Falls Church, Virginia

Antenna Section
Naval Air Missile Test Center
Point Mugu, California

L. Fahnestock
Fairchild Engine & Airplane Corp.
Fairchild Airplane Division
M/F Contract AF33(038)-18499
Hagerstown, Maryland

Mr. A. Kandoian
Federal Telecommunications Lab.
M/F Contract AF33(616)-3071
500 Washington Avenue
Nutley 10, New Jersey

Ryan Aeronautical Company
Lindbergh Drive
M/F Contract W-33(038)ac-21370
San Diego 12, California

Mr. Thatcher
Republic Aviation Corporation
M/F Contract AF18(600)-1602
Hicksville, Long Island, New York

Dr. C. H. Papas
Dept. of Electrical Engineering
California Institute of Technology
Pasadena, California

Lockheed Aircraft Corporation
Missile Systems Division
ATTN: E. A. Blasi
Department 54-12, Building 130
M/F Contract AF33(616)-6022
Sunnyvale, California

General Electric Co.
French Road
ATTN: Mr. Grimm, LMEED
M/F Contract AF33(600)-30632
Utica, New York

D.E. Royal
The Ramo-Wooldridge Corp.
Communications Division
P.O. Box 45444
Airport Station
Los Angeles 45, California

Mr. A. W. Boekelheide
Motorola, Inc.
Defense Systems Lab.
M/F Contract NOa(s)-53-492-c
3102 N. 56th Street
Phoenix, Arizona

Stanford Research Institute
Southern California Laboratories
ATTN: Document Librarian
820 Mission Street
Contract AF19(604)-1296
South Pasadena, California

Professor J. R. Whinnery
Department of Electrical Engineering
University of California
Berkeley, California

Professor Morris Kline
Mathematics Research Group
New York University
45 Astor Place
New York, New York

Professor A. A. Oliner
Microwave Research Institute
Polytechnic Institute of Brooklyn
55 Johnson Street - Third Floor
Brooklyn, New York

DISTRIBUTION LIST (CONTINUED)

Antenna Department
Radiation, Inc.
Technical Library Section
M/F Contract AF33(600)-36705
Melbourne, Florida

Electronics Division
Westinghouse Electric Corporation
M/F Contract AF33(600)-27852
Friendship International Airport
Box 746
Baltimore 3, Maryland

Rex Beam
Ta-Mar, Incorporated
M/F Contract AF33(604)-18651
2339 Cotner Avenue
Los Angeles 64, California

R. C. Huntington
Motorola, Inc.
8201 E. McDowell Road
Phoenix, Arizona

Dr. T. E. Tice
Ohio State Univ. Research Foundation
1314 Kinnear Road
Columbus 8, Ohio

J. B. Smyth
Smyth Research Associates
3555 Aero Court
San Diego 11, California

Army Rocket and Guided Missile Agency
U.S. Army Ordnance Missile Agency
ATTN: ORDXR-OMR
Redstone Arsenal, Alabama